CHAPTER VI

PSS doped PEDOT functionalized with *f*MWCNTs for the detection of Aflatoxin B_1, Organophosphate and Carbamate

In this work the multi-component matrix based on PEDOT, PSS and fMWCNTs has been synthesized as a biosensor probe to immobilize anti-AFB_1 and AChE. The morphological, structural and electrochemical properties of the synthesized PEDOT-PSS, PEDOT-PSS-fMWCNTs, BSA/anti-AFB_1/PEDOT-PSS-fMWCNTs and AChE/PEDOT-PSS-fMWCNTs electrode systems have been carried out using FESEM, FTIR, cyclic voltammetry and electrochemical impedance spectroscopy. A relative study of all modified electrodes has been conducted and sensing of the bioelectrodes towards respective analytes has been performed using DPV. The biosensor parameters viz. linearity, sensitivity, incubation time, limit of detection and limit of quantification have been determined. The performance of synthesized biosensors towards the real samples has been tested to verify its feasibility.

6.1 Introduction:

Poly (3, 4-ethylenedioxythiophene) is a conducting polymer (CP) with the largest prospects in the field of biosensing due to unique combination of its characteristics (conductivity, stability, transparency and biocompatibility) [418, 419] and it can be functionalized further to increase its processability [420]. In this chapter PEDOT-PSS films have been synthesized by electrochemical polymerization of EDOT in poly- (styrenesulfonic acid) (PSS) solution to give a PEDOT-PSS film. The conjugated polymer PEDOT is positively doped and the sulfonyl groups which are de-protonated carrying negative charge of PSS which act as the 'counterions' and it is used to balance the doping charges [421]. PEDOT-PSS films are almost transparent and highly stable, which is a promising characteristic for electrode fabrication for bio-sensing applications [421, 422].

A secondary dopant is a substance which is used for enhancement in conductivity of a primarily doped conjugated polymer and the incorporation of secondary dopant results in a synergistic effect [423]. Even after complete removal of the secondary dopants the enhanced properties of the polymer may persist [424, 425].

In this chapter multi walled carbon nanotubes have been used as the secondary dopants to improvise the properties of PEDOT-PSS like poor conductivity. Carbon nanotubes (SWCNTs or MWCNTs) have been extensively used in a biosensor electrode due to its excellent conductivity, low specific weight, ideal specific surface area and chemical stability [426, 427]. Among them functionalized multiwalled carbon nanotubes (*f*MWCNTs) have sparkled much attention as sensing element which enhances the transfer of electrodes during the bio-electrochemical reaction due to the high aspect ratio ability to provide high external surface area and promote electron transfer, high sensitivity, low limit of detection and chemical stability [428]. Functionalization of MWCNTs with carboxyl group is one of the widely used strategies to increase their water dispersibility and ability to conjugate with various molecules for the desired applications. Moreover the acid treatment provides functional groups COOH which helps in forming covalent bond with the NH_2 group of the biomolecule [429, 430].

A multi nanocomposite based on Poly (3, 4-ethylenedioxythiophene) (PEDOT), Polystyrene sulfonate (PSS) and functionalized multi walled carbon nanotubes (*f*MWCNTs) has been developed. Thin film of PEDOT-PSS has been controllably deposited on a substrate surface via the application of an optimized potential sufficient to oxidize and polymerize its monomer EDOT. Incorporation of *f*MWCNTs will enhance the properties of the PEDOT-PSS composite and the synergic effect of all the components results in achieving a biosensor electrode with improved parameters. The electrode PEDOT-PSS-*f*MWCNTs has been used to immobilize anti-AFB_1 for the detection of AFB_1 and AChE for the detection of aflatoxin B_1, methyl parathion and carbofuran. Similar to Methyl parathion, Carbofuran is a toxic insecticide which belongs to carbamate group and it an AChE inhibitor. It has been used to control the growth of insects in wide variety of field crop.

Morphological studies were carried out by Field emission Scanning Electron Microscope (JEOL-JSM-6390LV). Contact angle measurements were made by Degree of Hydrophilicity measurement set up (Model: DSA 15B). The FT-IR spectrum (Spectrum 100 with software version CPU32) was used for the conformational studies. All the electrochemical measurements, viz. cyclic voltammetry, impedance spectroscopy and Differential pulse voltammetry were performed using a Potentiostat/Galvanostat/ZRA (Gamry Reference 3000, USA) with Gamry Echem Analyst Software. Glassy carbon electrode, Ag/AgCl (3 M KCl) and a platinum wire were used as working, reference and auxiliary electrodes, respectively. The cyclic voltammetry and impedance spectroscopy measurements were performed in 100mM PBS containing 5mM $K_3[Fe(CN)_6]$ / $K_4[Fe(CN)_6]$ keeping 1:1 ratio as redox probe. The impedance spectra were measured in the frequency range from 10^6 Hz to 0.08 Hz at amplitude of 20mV vs. Ag/AgCl. The activity of BSA/anti-AFB_1/PEDOT-PSS-*f*MWCNTs/GCE and AChE/AuNPs/PEDOT-PSS-*f*MWCNTs/GCE electrodes towards respective analytes has been investigated using DPV technique.

6.2 Morphological Analysis:

The surface morphologies of the different modified electrodes before and after immobilization were investigated by FESEM (Figure 6.1). The image corresponding to PEDOT-PSS polymeric film represents a rough, porous network with heterogeneous grains. After doping with *f*MWCNTs, the surface roughness decrease and they are wrapped in the growing polymer and an interconnected network of nanotubes may have formed (shown by red pointer). The immobilization of anti-AFB1 results in a fuzzy surface with distribution of indistinguishable particles Figure 6.1 (C). After covalent immobilization of AChE (Figure 6.1 (D)), the porosity of the film increases and the surface alters to a more regular globular structure due to the presence of AChE molecules indicating the adequate and satisfactory immobilization of AChE onto surface of the prepared nanocomposites.

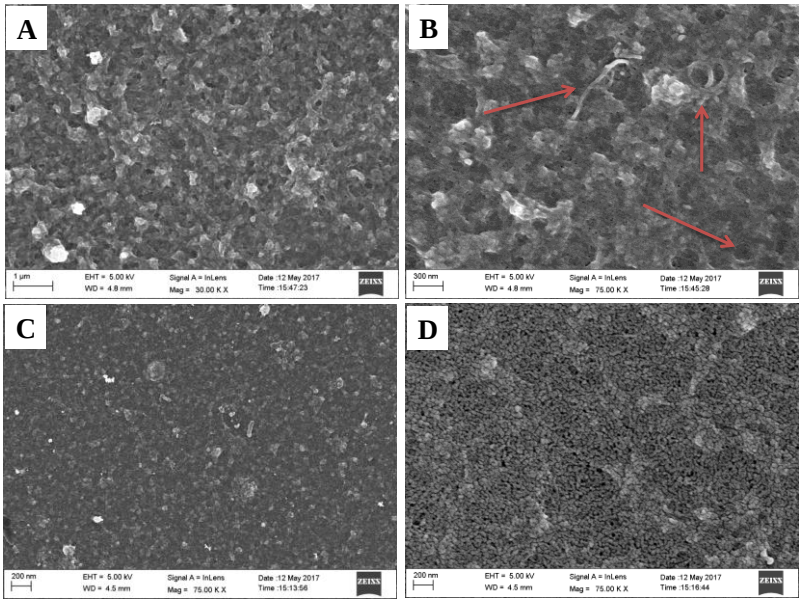

Figure 6.1: FESEM Micrograph of (A) PEDOT-PSS- film, (B) PEDOT-PSS-*f*MWCNTs, (C) BSA/anti-AFB_1/PEDOT-PSS-*f*MWCNTs film and (D) AChE/PEDOT-PSS-*f*MWCNTs film

6.3 Contact Angle Measurements:

The study of molecular interaction of water droplets in the liquid solid interface has been done by the contact angle (CA) measurement. It is based on the classical liquid-solid-vapor interaction model and the angle is given by [431]:

$$\cos\theta_c = \frac{\vartheta_{SG} - \vartheta_{SL}}{\vartheta_{LG}} \qquad 6.1$$

where ν_{sg} and ν_{lg} is the solid-liquid interfacial energy and liquid- vapor interfacial energy, θ_C is the equilibrium contact angle. Figure 6.2 shows contact angle of 6 µL of DD water drop on PEDOT-PSS and PEDOT-PSS-*f*MWCNTs films before immobilization of protein. The values of contact angle are found to be 59^0 and 44^0 ($<90^0$) which is characteristic of hydrophilic nature of the film [432].The presence of functional groups in the *f*MWCNTs results in more hydrophilic nature of PEDOT-PSS-*f*MWCNTs matrix making the film more suitable for anti-AFB_1 and AChE immobilization. The volume of water droplet decreases more in case of PEDOT-PSS-*f*MWCNTs which indicates that the interaction of hydrophilic molecule of the PEDOT-PSS-*f*MWCNTs film with water is thermodynamically more favorable [432]. The protein immobilization requires a hydrophilic surface since their structural conformation might get change as the protein loses its β-sheets configuration at hydrophobic surfaces. The hydrophobicity of surface contributes to

unwanted interactions between the proteins and the matrix, which could create a problem with unspecific binding [355].

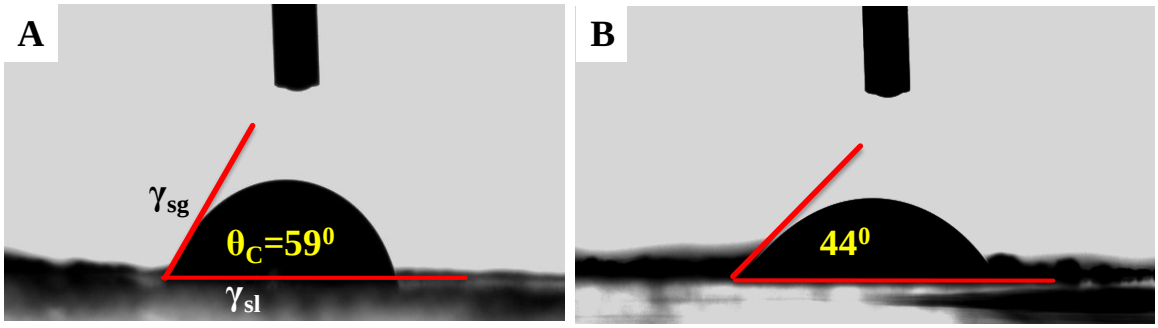

Figure 6.2: Contact angle measurement of (A) PEDOT-PSS and (B) PEDOT-PSS-*f*MWCNTs film.

6.4 FTIR Spectroscopy:

FTIR has been done to study the fundamental stretching vibrations of PEDOT-PSS, PEDOT-PSS-*f*MWCNTs and BSA/anti-AFB_1/PEDOT-PSS-*f*MWCNTs as shown in Fig. 3. The vibrations between 1350 cm^{-1} and 1600 cm^{-1} are assigned to thiophene rings, phenyl rings and quinoidal structure in PEDOT and PSS [433, 434].

The absorption band specifically the C-O-C stretching band at 1070 cm^{-1} can be used to recognize PEDOT. The peak at 670 cm^{-1} is assigned to the C-S-C bond stretching in the thiophene ring [435] and the vibrations at 1180 cm^{-1} and 1030 cm^{-1} are assigned to S=O and O-S-O vibrations in PSS [436]. After doping with MWCNTs, the peak of PEDOT-PSS-*f*MWCNTs appeared at 3400 cm^{-1} and 2930 cm^{-1} due to the presence of OH stretching vibrations and C-H_2 indicating the presence of SP^3 defects [437, 438]. The bands 1490 cm^{-1} and 1690 cm^{-1} are the indication of functionalization and activation of the COOH onto the surface of MWCNTs. Moreover the peaks at 1090 cm^{-1} and 910 cm^{-1} indicates the deformation of C-O-C and the oxyethylene ring which indicates that MWCNTs being wrapped inside the PEDOT polymer [439].

The peak of N-H bending for primary amine at 1657 cm^{-1} is observed in the FTIR spectrum of BSA/anti-AFB_1/PEDOT-PSS-*f*MWCNTs and the vibration at 826 cm^{-1} which confirms the bonding of anti-AFB_1 with the matrix of PEDOT-PSS-*f*MWCNTs [440].

The FTIR spectrum of AChE enzyme shows two vibration peaks between 1600 cm^{-1} and 1690 cm^{-1} which correspond to the amide I and amide II groups of the proteins [441]. This shows that the AChE immobilized on PEDOT-PSS-*f*MWCNTs retained its native structure.

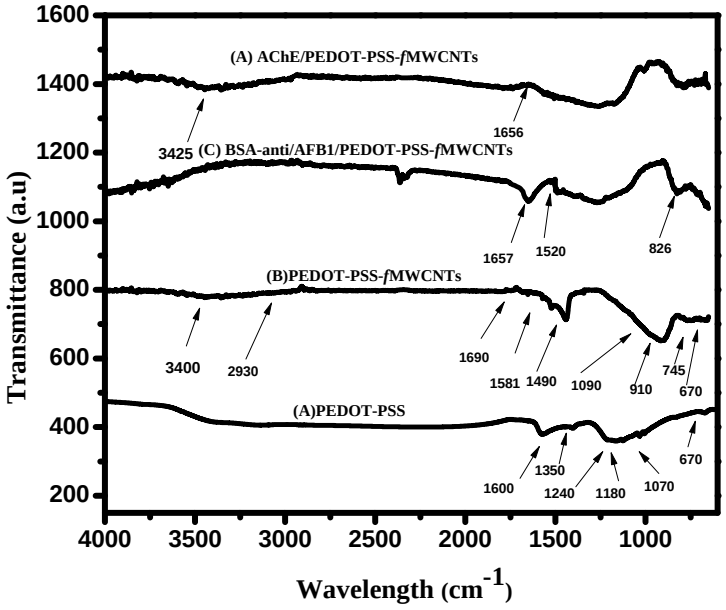

Figure 6.3: FTIR spectra of (A) PEDOT-PSS/GCE, (B) PEDOT-PSS-*f*MWCNTs/GCE, (C) BSA/anti-AFB_1/PEDOT-PSS-*f*MWCNTs/GCE and (d) AChE/PEDOT-PSS-*f*MWCNTs/GCE.

6.5 Electrochemical Impedance Spectroscopy:

The information of membrane capacitance and resistance can be investigated using EIS technique and the Nyquist complex plane plots of all the electrodes exhibits a typical impedance spectrum of the modified electrodes, demonstrating a well-defined a single semicircle at high frequency domain and a straight line at low frequency domain. The linear tail with a slope of unity is dominated by the interfacial mass transfer of the redox species, while the semicircular impedance is mainly contributed by the charge-transfer resistance (R_{ct}) and the double-layer capacitance (C_{dl}) of the electrode surface [360].

Figure 6.4 (A) displays the Nyquist Plot of GCE, PEDOT-PSS/GCE, PEDOT-PSS-*f*MWCNTs/GCE, BSA/anti-AFB_1/PEDOT-PSS-*f*MWCNTs/GCE and AChE/PEDOT-PSS-*f*MWCNTs/GCE. At high frequencies $Z(\omega) = Z'(\omega) = R_s$, as the frequency dependent term vanishes and R_s = 41.35 Ω (for PEDOT-PSS-

*f*MWCNTs/GCE), the intercept on the Z´ (ω) axis on the high-frequency side where Z″ (ω) = 0.

Similarly at lower frequency side (For ω → 0), Z (ω) is sum total of $R_s + R_p$= 181 Ω, which is the intercept on the Z´ (ω) axis on the low frequency side.

Analogous information is obtained by examining the Bode diagram (Figure 6.4 (B)) where Log R_s and Log (R_p+R_s) are obtained straight forwardly from the Z (ω) versus log ω plot at high and low frequencies. The values of R_{et} and C_{dl} calculated using equation 6.1 and 6.2 derived from Nyquist Plot and Bode plot have been tabulated in Table 6.1.

$$R_{et} = (R_p + R_s) - R_s \quad 6.1$$

$$C_{dl} = \frac{1}{2\pi f_{max} R_{et}} \quad 6.2$$

The resistance to the flow of electron in PEDOT-PSS/GCE (R_{et} ~ 380 Ω) and GCE (R_{et} ~ 486 Ω) is found to be more or less comparable. This may be due the poor conduction of PEDOT-PSS as result of which no dramatic decrease in the R_{et} occurs after modification GCE with PEDOT-PSS composite. The activation barrier is found to be minimum for PEDOT-PSS-*f*MWCNTs/GCE (R_{et} ~140 Ω) and should be noted that introduction of the *f*MWCNTs significantly decreased the R_{et} value, owing to the enhanced electron transfer by increasing interfacial catalytic active sites between PEDOT-PSS-*f*MWCNTs/GCE electrode and the redox active solution ($Fe[(CN)_6]^{3-/4-}$). The R_{et} value increases to ca. 865 Ω and 787 Ω for BSA/anti-AFB_1/PEDOT-PSS-*f*MWCNTs/GCE and AChE/PEDOT-PSS-*f*MWCNTs/GCE, respectively. It implies the capacitive behavior of protein immobilized electrodes due to assemblance of non conducting species [442] over the interface of PEDOT-PSS-*f*MWCNTs and electrolyte which hinders the flow of electrons (Fe(IV)/Fe(III)). The Φ versus log ω plot as shown in Figure 6.4 (C) shows that the impedance responses of all modified electrodes are resistive primarily at high and low frequencies, whereas at intermediate frequencies, BSA/anti-AFB_1/PEDOT-PSS-*f*MWCNTs/GCE and AChE/PEDOT-PSS-*f*MWCNTs/GCE becomes capacitive as their phase shifts get closer to 90^o [231].

Table 6.1: The calculated value of R_{et}, C_{dl} and Φ for the modified electrodes.

Electrode	R_{et}(Ω)	C_{dl} (F)	Φ(^{0}) (-ve)
GCE	486	1.45×10^{-4}	32
PEDOT-PSS/GCE	380	2.46×10^{-7}	25.8
PEDOT-PSS-*f*MWCNTs/GCE	141	2.78×10^{-6}	12
BSA/anti-AFB_1/ PEDOT-PSS-*f*MWCNTs/GCE	865	1.79×10^{-4}	42.87
AChE/PEDOT-PSS-*f*MWCNTs	787	2.17×10^{-4}	48

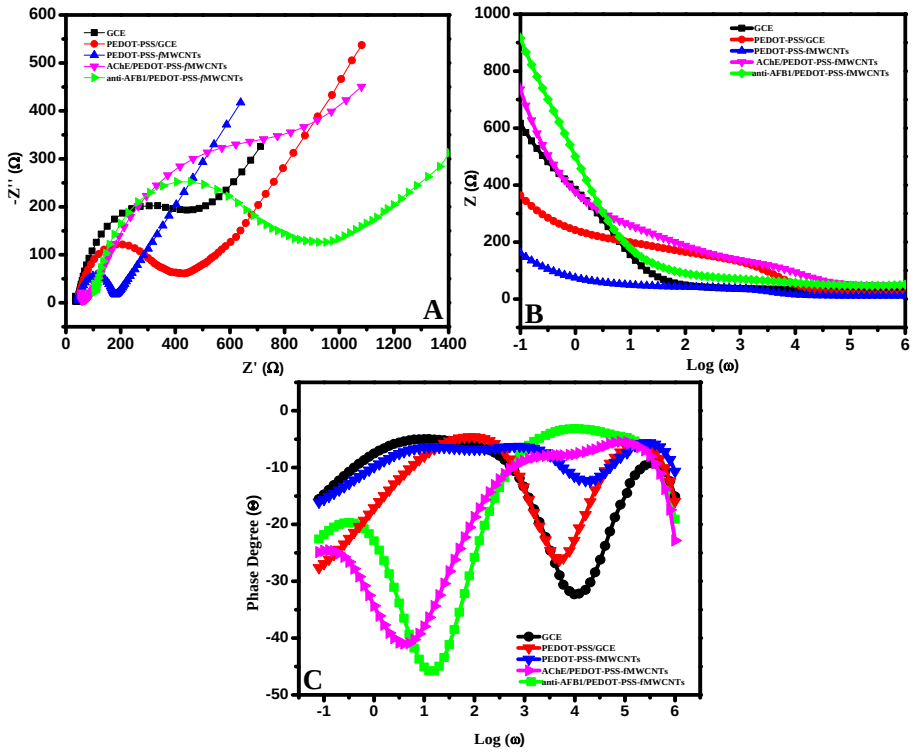

Figure 6.4 : EIS pattern of all modified electrodes (A) Nyquist Plot (Z′ vs. -Z″), (B) Bode plot (Z vs. Log ω) and (C) Phase shifts in 100mM PBS and 5mM $[Fe(CN)_6]^{3-/4-}$.

6.6 Cyclic Voltammetry Studies:

6.6.1 Electrocatalytic behaviour of modified electrodes towards redox species:

The electrochemical behavior of the modified electrodes towards the oxidation and reduction reaction of electro-active species $[Fe(3+) \leftrightarrow Fe(4+) + e']$ has been studied using cyclic voltammetry. The cyclic voltammogram (CV) of (a) GCE, (b) PEDOT-PSS/GCE and (c) PEDOT-PSS-*f*MWCNTs/GCE in a solution containing 100mM PBS (pH 7.4) and 5.0 mM $[Fe(CN)_6]^{3-/4-}$ as a redox probe at a scan rate of 5 mV $s^{-1}$is displayed in Figure 6.5 (A). The CV of all electrodes shows characteristics peaks due to the diffusion layer near the electrodes and since the electrodes act as an oxidant (reductant) and the oxidation (reduction) current increases to a peak. Therefore the catalytic behavior of the electrodes towards $[Fe(CN)_6]^{3-/4-}$ is based on the variation of anodic (I_{pa}) and cathodic peak (I_{pc}) currents and location of forward and reverse peaks on the potential axis (E_{pa} and E_{pc} and ΔE_p) within a wide potential range vs. Ag/AgCl. All the electrodes show noticeable redox peaks and the high intensity oxidation and reduction peak current density suggests an improved electro-reductive behavior to Fe(IV)/Fe(III) redox couple. The value of ΔE_p suggest mechanism of the reaction of electrode and the electrolyte from reversible (ΔE_p= 59 mV) to quasi reversible (59 mV$\leq \Delta E_p \leq$ 200 mV) one [243]. As the surface of GCE has been modified with PEDOT-PSS-*f*MWCNTs the peak current intensity increases from 21 µA to 169 µA (anodic) and -23 µA to -168 µA (cathodic), respectively. Moreover the ratio of forward and reverse current ($\frac{I_{pa}}{I_{pc}} \sim 1$) is equivalent to one which denotes the stability of the product on the time scale of the experiment. This behavior of PEDOT-PSS-*f*MWCNTs suggests an improved electrochemical property and it can be ascribed to the synergic effect of PEDOT-PSS and *f*MWCNTs. The existence of *f*MWCNTs can accelerate the transfer of electron and enhance the sensitivity of response due to their good active surface, catalytic properties and excellent conductivity [443]. The decreased value of ΔE_p for PEDOT-PSS-*f*MWCNTs suggests fast electron transfer mechanism as the value (69 mV) is more towards the standard value of reversible reaction (59 mV) [243]. Figure 6.5 (B) shows the cyclic voltammogram of PEDOT-PSS-*f*MWCNTs after immobilization of anti-AFB_1 and AChE and the deposition of non conducting protein may obstruct the

flow of electron as the interface behaves as capacitor which can be correlated with EIS results (Section 6.5).

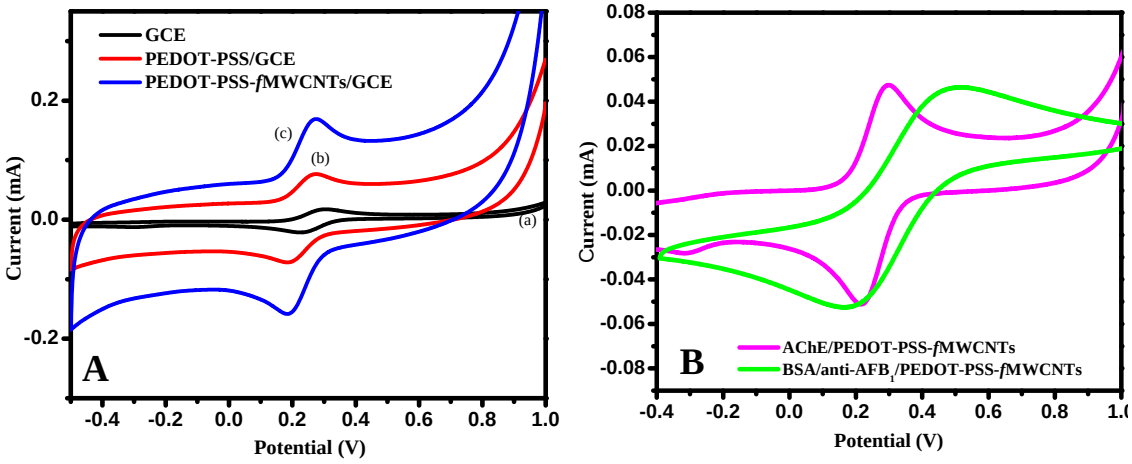

Figure 6.5: The CV patterns of bare (A) (a) GCE, (b) PEDOT-PSS/GCE and (c) PEDOT-PSS-*f*MWCNTs/GCE (B) The CV of BSA/anti-AFB_1/ PEDOT-PSS-*f*MWCNTs/GCE and AChE/ PEDOT-PSS-*f*MWCNTs/GCE in 100mM PBS (pH 7.2) and 5mM $[Fe(CN)_6]^{3-/4-}$ at 15 mV/s vs. Ag/AgCl.

Table 6.2: The parameters of cyclic voltammogram (I_{pa} and I_{pc} and ΔE_p) for the modified electrodes at 15 mV/s vs. Ag/AgCl.

Electrodes	**I_{pa}**	**I_{pc}**	**$\Delta E_p(E_{pa}-E_{pc})$ mV)**
GCE	0.0153	-0.022	0.083
PEDOT-PSS	0.077	-0.0724	0.071
PEDOT-PSS-*f*MWCNTs	0.169	-0.168	0.069
AChE/PEDOT-PSS-*f*MWCNTs	0.044	-0.0527	0.097
BSA/anti-AFB_1/PEDOT-PSS-*f*MWCNTs	0.046	-0.052	0.261

6.6.2 Variation of Anodic (I_{pa}) and Cathodic Current (I_{pc}) vs. Scan rate (v):

Figure 6.6 shows the variation of cyclic voltammogram (CV) of PEDOT-PSS/GCE, PEDOT-PSS-*f*MWCNTs/GCE, BSA/anti-AFB_1/PEDOT-PSS-*f*MWCNTs/GCE and AChE/PEDOT-PSS-*f*MWCNTs/GCE with increasing scan rate from 5mV/s to 30mV/s vs. Ag/AgCl. The total current density in cyclic voltammetry is given by [444]:

$$J_p = \left[2.72 \times 10^5 n^{\frac{3}{2}} D^{\frac{1}{2}} C^b\right] \vartheta^{\frac{1}{2}} : J = J_f + C_d \frac{dE}{dt} \qquad 6.3$$

where J_p is the total current density, n is the number if electron transfer, J_f is the faradaic current, C_d is the double layer capacitance and D is the diffusion coefficient, respectively. The peak current in CV pattern of the electrodes is due to faradaic current at lower scan rate but as the scan rate increases capacitive current increases. If the rate depends exclusively on the spontaneous diffusion of the electro-active species then it is called diffusion controlled electrode reaction [237]. The changing value of peak current intensity (I_{pa} and I_{pc}) versus square root of scan rate ($\nu^{1/2}$) of all electrodes is shown in Figure 6.7 and there is a linear variation of current with $\nu^{1/2}$($I \propto \nu^{1/2}$). It implies the electrode- electrolyte reaction is diffusion controlled process and the current depend on the concentration of (Fe(IV)/Fe(III)) according Randles Sevcik theory [237, 238] and no specific interaction is occurring between the redox species.

The regression equation of the linear plot of PEDOT-PSS/GCE and PEDOT-PSS-*f*MWCNTs/GCE is given by equation 6.4 and 6.5 and the values of slopes and regression coefficient are tabulated in Table 6.3:

$$I_{pa}(mA) = 1.2 \times v^{\frac{1}{2}} + (-0.03);\ I_{pc}(mA) = -0.9 \times v^{\frac{1}{2}} + (-0.036) \qquad 6.4$$

$$I_{pa}(mA) = 02.9 \times v^{\frac{1}{2}} + (-0.16);\ I_{pc}(mA) = -2.7 \times v^{\frac{1}{2}} + (-0.15) \qquad 6.5$$

According to Randles Sevcik theory [237, 238] the linearity slope can be used to calculate the electro active surface area of the modified electrode using the equation:

$$I_p = 0.446\, nFAC \left(\frac{nF\nu D}{RT}\right)^{1/2} \qquad 6.6$$

where F is the Faraday's constant, A is the electro active area, C and D is the concentration and diffusion coefficient of redox species, R is the gas constant and T is the room temperature. The value of electro-active area (Table 6.4) of PEDOT-PSS-*f*MWCNTs /GCE is higher as compared to PEDOT-PSS/GCE which is attributed the presence of carbon nanotubes with large surface area of about 1315 m^2/g (theoretical value) and high porosity of the hybrid. Therefore the carbon nanotubes incorporated PEDOT-PSS matrix is considered as an ideal electrode for the immobilization of the bioreceptors.

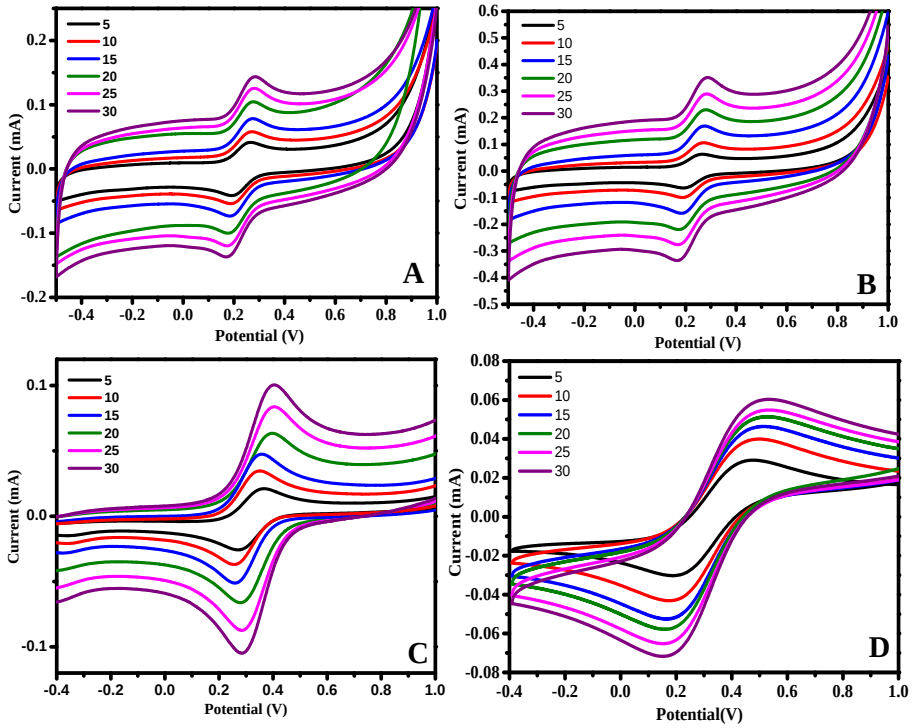

Figure 6.6: The Cyclic Voltammogram of (A) PEDOT-PSS/GCE (B) PEDOT-PSS-*f*MWCNTs/GCE, (C) AChE/PEDOT-PSS-*f*MWCNTs/GCE and (D) BSA/anti-AFB_1/PEDOT-PSS-*f*MWCNTs/GCE in 100mM PBS (pH 7.4) and 5mM $[Fe(CN)_6]^{3-/4-}$ at a scan rate ranging from 5 mV/s to 30 mV/s.

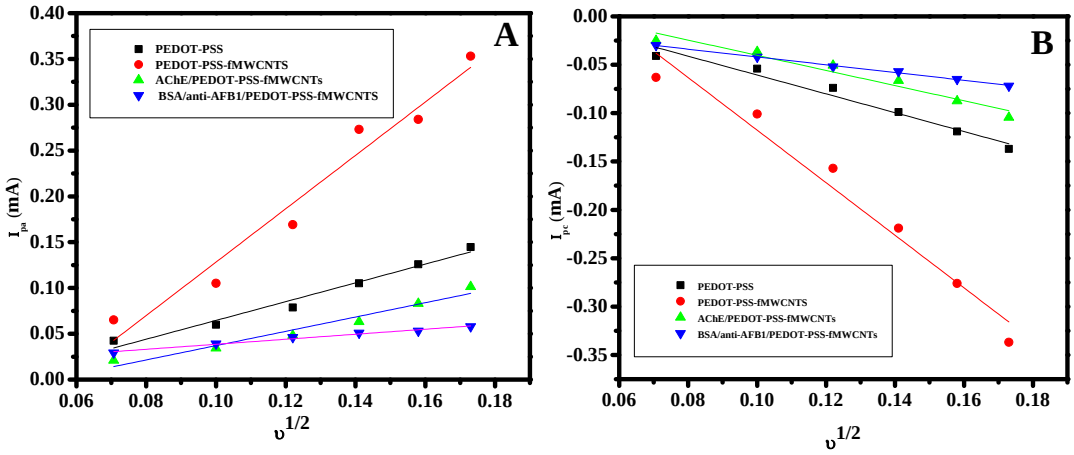

Figure 6.7: The variation of I_{pa} and I_{pc} of PEDOT-PSS/GCE, PEDOT-PSS-*f*MWCNTs/GCE, AChE/PEDOT-PSS-*f*MWCNTs/GCE and BSA/anti-AFB_1/PEDOT-PSS-*f*MWCNTs/GCE in 100mM PBS and 5mM $[Fe(CN)_6]^{3-/4-}$ with $v^{1/2}$ in V/s.

Table 6.3: The value of slope y-intercept and regression coefficient for variation of I_{pa} and I_{pc} with $\upsilon^{1/2}$.

Electrode	Anodic Slope	Cathodic slope	Regression coefficient
PEDOT-PSS	1.029	0.973	0.98
PEDOT-PSS-*f*MWCNTs	2.913	2.716	0.98
AChE/PEDOT-PSS-*f*MWCNTs	0.780	0.783	0.97
BSA/anti-AFB_1/PEDOT-PSS-*f*MWCNTs	0.273	0.401	0.99

Table 6.4: The calculated values of electro active surface area of modified electrodes.

Electrode	Electro-active area (cm^2)
GCE	0.09
PEDOT-PSS	0.21
PEDOT-PSS-*f*MWCNTs	0.818

After immobilization of the anti-AFB_1 and AChE on PEDOT-PSS-*f*MWCNTs/GCE, the change in the value of peak current with respect to the scan rate has been plotted

for BSA/anti-AFB_1/PEDOT-PSS-*f*MWCNTs/GCE and displayed in Figure 6.8. The slopes of the linearity plot have been used to calculate the ionic species (I*) concentration using equation 6.7 and the value of I* is presented in Table 6.5.

$$I_p = \frac{n^2F^2I^*A\upsilon}{4RT} \qquad 6.7$$

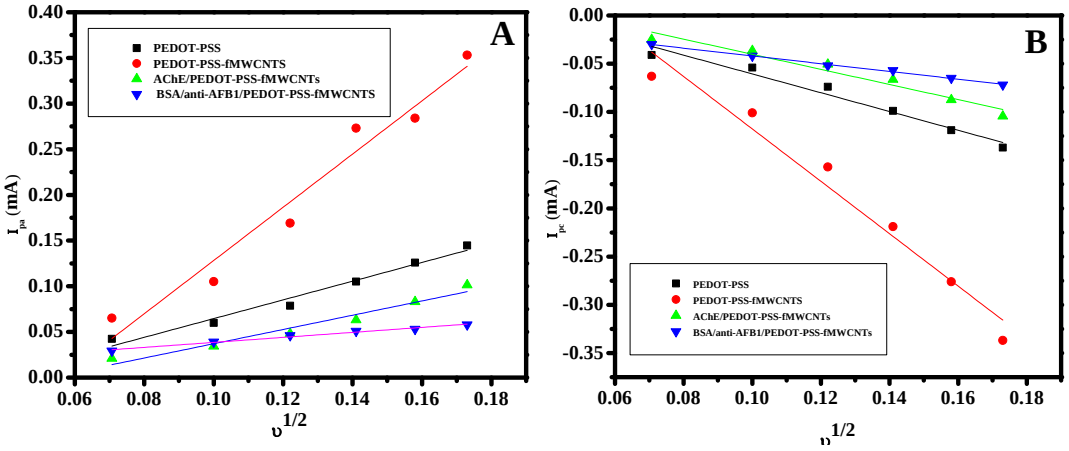

Figure 6.8: The variation of I_p of (A) BSA/anti-AFB_1/PEDOT-PSS-*f*MWCNTs/GCE and (B) AChE/PEDOT-PSS-*f*MWCNTs/GCE versus scan rate in V/s.

Table 6.5: The value of ionic species after immobilization anti-AFB_1 and AChE

Protein	**Surface concentration (I*) in PEDOT-PSS-*f*MWCNTs/GCE (molcm^{-2})**
anti-AFB_1	1.65×10^{-5}
AChE	4.9×10^{-5}

6.6.3 Variation of Anodic (E_{pa}) and Cathodic (E_{pc}) peak potential vs. scan rate (v):

Figure 6.8 shows the variation of E_{pa} and E_{pc} with respect to the Log of scan rate ranging from 50 mV/s to 75 mV/s of all the synthesized electrodes. The peak voltages do not alter as a function of scan rate in reversible reaction whereas the shifting in position of peak potential is a characteristic of quasi reversible process [239]. According to Laviron's method [254], the potentials varied linearly with scan

rate and the slopes of the plots have been analyzed to evaluate the value of α using equation 6.8 and 6.9 and heterogeneous rate constant k_s using equation 6.10, respectively.

$$Cathodic\ slope = -2.3RT\frac{log\upsilon}{\alpha nF} \quad 6.8$$

$$Anodic\ Slope = 2.3RT\frac{log\upsilon}{(1-\alpha)nF} \quad 6.9$$

$$logk_s = \alpha log(1-\alpha) + (1-\alpha)log\alpha - log\frac{Rt}{nvF} - \frac{\alpha(1-\alpha)nF\Delta E_p}{2.3RT} \quad 6.10$$

where *n* is the electron transfer number, R is the gas constant, T is the absolute temperature, and ΔE_p is the peak-to peak separation. The value of anodic and cathodic electron transfer coeficient (Table 6.6) of PEDOT-PSS-*f*MWCNTs/GCE is determined as 0.741 and 0.286, respectively. This results show that the rate limiting steps for cathodic and anodic might not be the same step. The mean value of k_s value for PEDOT-PSS-*f*MWCNTs/GCE is found to be 1.82×10^2 which indicates fast kinetics of the redox couple which may be due to the presence highly conducting network of carbon nanotubes across polymer matrix [443]. As presented in Table 6.6, the value of k_s obtained for all the electrodes falls in the quasi reversible reaction range of $0.020 > k_s > 5\times 10^{-5}$ [261]. The value of k_s after immobilization of proteins is found to be in order 10^{-2} which suggests that the electron transfer pathway of the protein behaved as a quasi-reversible system. Therefore we can consider PEDOT-PSS-*f*MWCNTs/GCE as a suitable electrode for immobilization of protein to achieve better performance with improved sensitivity. Figure 6.10 illustrates the linear variation of ΔE_p of all the modified electrodes with the scan rate showing a quasi reversible electrode mechanism [243]. In a quasi-reversible electron transfer reactions, ΔE_p shifts depending upon the voltage scan rate which occurs because the current takes more time to respond to the applied voltage than the reversible case.

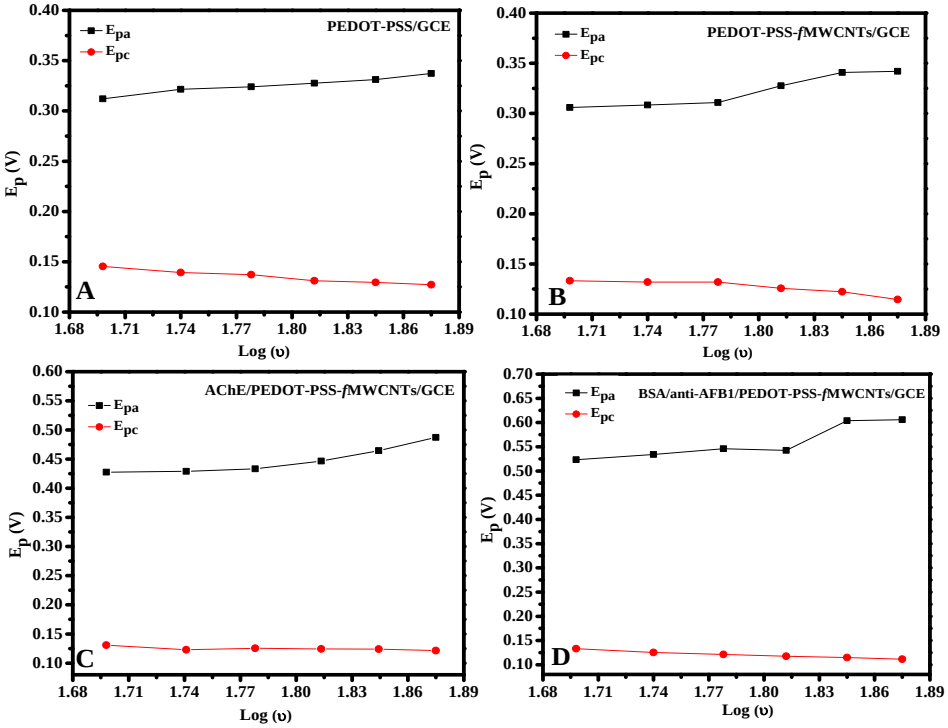

Figure 6.9: The variation of E_{pa} & E_{pc} of (A) PEDOT-PSS/GCE, (B) PEDOT-PSS-*f*MWCNTs/GCE (C) AChE/PEDOT-PSS-*f*MWCNTs/GCE and (D) BSA/anti-AFB_1/PEDOT-PSS-*f*MWCNTs/GCE with Log (ν) (50 mV/s to 75 mV/s).

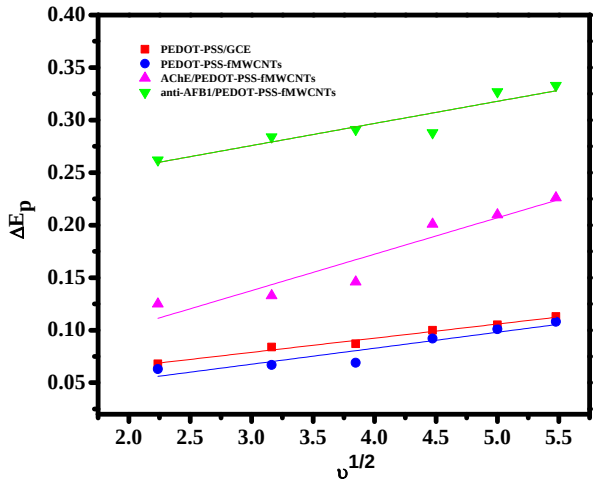

Figure 6.10: The variation of ΔE_p of PEDOT-PSS/GCE, PEDOT-PSS-*f*MWCNTs/GCE, AChE/PEDOT-PSS-*f*MWCNTs/GCE and BSA/anti-AFB_1/PEDOT-PSS-*f*MWCNTs/GCE with $\nu^{1/2}$ (5 mV/s to 30 mV/s).

Table 6.6: The calculated values of heterogeneous rate transfer constant (k_s) and transfer coefficient (α).

Electrode	k_s (s^{-1})	α
PEDOT-PSS/GCE	1.9×10^{-1}	0.55
PEDOT-PSS-*f*MWCNTs/GCE	1.82×10^{2}	0.53
BSA/anti-AFB_1/PEDOT-PSS-*f*MWCNTs/GCE	5.7×10^{-1}	0.37
AChE/PEDOT-PSS-*f*MWCNTs/GCE	2.9×10^{-1}	0.41

6.7 Application of BSA/anti-AFB_1/PEDOT-PSS-fMWCNTs/GCE to detect AFB_1:

6.7.1 Optimization of Experimental parameters:

We have optimized the electrode stability, incubation time and pH of the standard solution to achieve maximum sensitivity of the immunosensor. It is important to study the stability after immobilization of the anti-AFB_1 in order to confirm whether the decrease in current during immune reaction is due to interaction of antigen & antibody, not due to poor stability of the BSA/anti-AFB_1/PEDOT-PSS-*f*MWCNTs/GCE. The incubation time of antigen and antibody interaction is a significant factor as the maximum current signal requires optimum incubation time. The most favorable condition for immune reaction has been achieved by maintaining the optimal pH of the reaction solution.

6.7.1.1 Electrochemical stability of the BSA/anti-AFB_1/PEDOT-PSS-fMWCNTs/GCE before and after immobilization:

The Cyclic Voltammetry studies of PEDOT-PSS-*f*MWCNTs in 100mM PBS and 5mM $[Fe(CN)_6]^{3-/4-}$ at a scan rate of 5 mV/s for 20 cycles have been done in order to study the electrochemical stability before of anti-AFB_1(Figure 6.11 (A)). The area of CV remains constant indicating no remarkable degradation of current with potential up to 20 cycles which may be due to the stable composite of PEDOT and PSS. After immobilization of anti-AFB_1, the same experiment has been performed as shown in Figure 6.11 (B) and there is no decrease in the peak current intensity (I_{pa} & I_{pc}) towards redox reaction of Fe (IV)/Fe (III) for 20 consecutive cycles which shows an excellent stability. Therefore the decrease in peak current after incubation of BSA/anti-AFB_1/PEDOT-PSS-*f*MWCNTs/GCE in AFB_1 solution is due to the

formation of antigen-antibody complex which hinders the flow of electrons between electrode and electrolyte.

6.7.1.2 Optimization of pH of the standard solution and the incubation time:

The Cyclic Voltammetry of the electrodes before immobilization Figure 6.12(A) has been performed at different pH ranging from 6.4 to 7.8 in order to study the performance of the electrode in an acidic or basic medium. The sensitivity of the electrode towards the redox reaction of Fe (IV)/Fe (III) is found to be maximum for pH 7.2. After immobilization of anti-AFB_1, the activity of BSA/anti-AFB_1/PEDOT-PSS-*f*MWCNTs in 100mM PBS and 5mM $Fe[(CN)_6]^{3-/4}$ (pH 6.4 to 7.8) in presence of 15 ng/mL AFB_1 (Figure 6.12 (B)) to find out the optimum pH for the antigen sensing. The maximum decrease in the DPV peak current signal is found in pH 7.2 which denotes maximum interaction antibody and antigen. The corresponding EIS results have been depicted in Figure 6.12 (C), which are consistent with the DPV results. The formation of the immune-reaction complex which has been accumulated in the surface of working electrode results in increase in R_{et} value is also found to be maximum at pH 7.2. This may be due to the fact that at highly acidic and highly alkaline environment, the antibodies may lose their binding ability with the antigen [179]. The result implies that the interaction of immobilized AFB_1 with the immunospecies occurs more effectively at pH 7.2.

The time required for the immune-reaction has been optimized by measuring DPV peak current of BSA/anti-AFB_1/PEDOT-PSS-*f*MWCNTs in absence and in presence of 15 ng/mL of AFB_1. Figure 6.13 (A) depicts that the DPV peak current decreases confirming maximum interaction with AFB_1 till 5 min and Figure 6.13 (B) shows variation of ΔI (I_0-I_i) with time in minute. Thus 5 min was chosen as the optimized incubation time required for antigen and antibody interaction in the successive experiments. All the experiments were performed in room temperature.

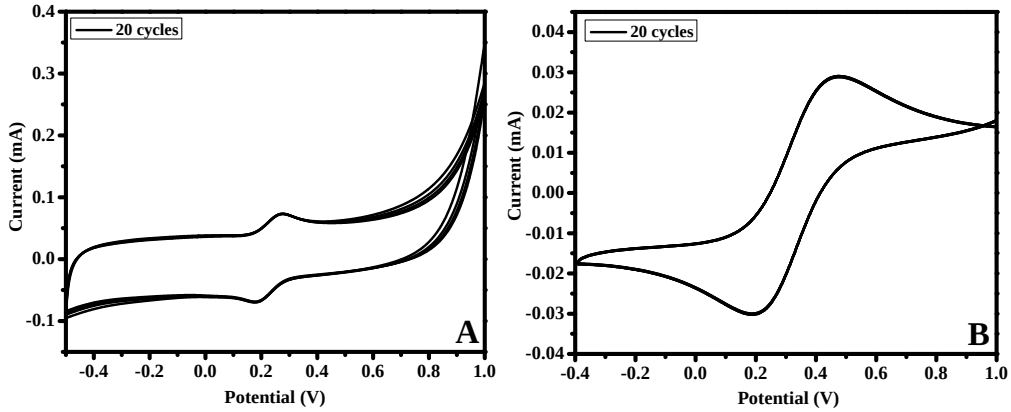

Figure 6.11: Cyclic voltammogram of (A) PEDOT-PSS-*f*MWCNTs and (B) BSA/anti-AFB$_1$/ PEDOT-PSS-*f*MWCNTs in 100mM PBS and 5mM Fe[(CN)$_6$]$^{3-/4}$ at 5mV/s vs. Ag/AgCl.

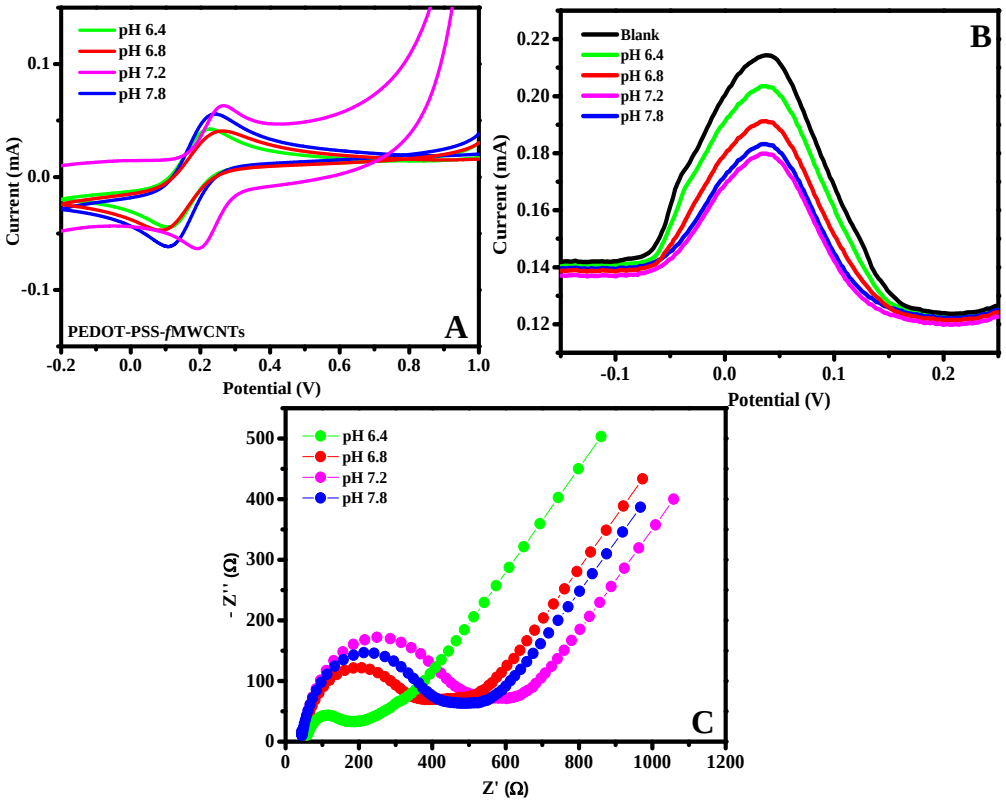

Figure 6.12: (A) The Cyclic voltammogram of PEDOT-PSS-*f*MWCNTs/GCE (B) DPV studies of BSA/anti-AFB$_1$/PEDOT-PSS-*f*MWCNTs/GCE (C) Nyquist Plot of BSA/anti-AFB$_1$/PEDOT-PSS-*f*MWCNTs/GCE in a solution containing 100mM PBS (pH 7.4) and 5mM [Fe(CN)$_6$]$^{3-/4-}$ with pH ranging from 6.4 to 7.8.

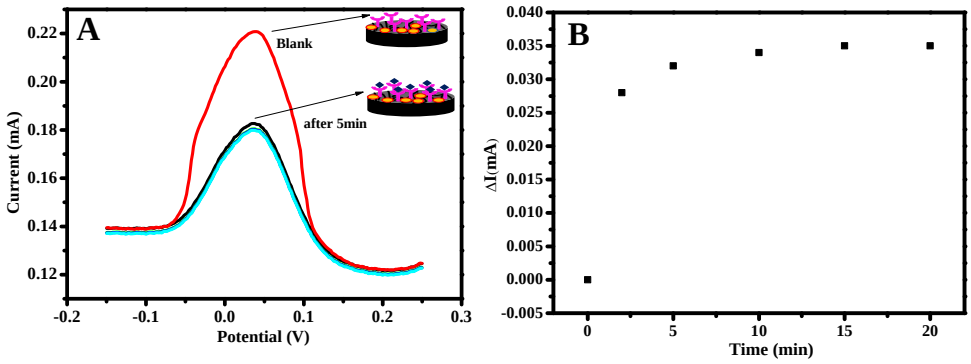

Figure 6.13: The variation of current in DPV of BSA/anti-AFB_1/PEDOT-PSS-*f*MWCNTs in 100mM PBS (pH 7.2) and 5mM $Fe(CN)_6^{3-/4-}$ containing 15 ng/mL AFB_1 after different incubation time (B) The variation of ΔI with time in min.

6.7.2 Analytical Performance of the BSA/anti-AFB_1/PEDOT-PSS-fMWCNTs/GCE towards detection of AFB_1:

The electrochemical response of immunoelectrode towards the redox reaction of Fe (III)/Fe (II) in presence of different concentration of AFB_1 has been studied by performing DPV of BSA/anti-AFB_1/PEDOT-PSS-*f*MWCNTs/GCE in 100mM PBS and 5mM $[Fe(CN)_6]^{3-/4-}$ containing different concentration of AFB_1 (0.1 to 75 ng/mL) (Figure 6.14 (A)). The DPV current peak decreases gradually with increasing concentration of AFB_1 indicating effective binding of AFB_1 with the active site of anti-AFB_1. As mentioned earlier assemblance of non conducting antigen-antibody complex obstruct the electron transfer between $[Fe(CN)_6]^{3-/4-}$ redox probe and the electrode [445]. The calibrated curve of ΔI (I_0-I_i) vs. concentration is shown in Figure 6.14 (B) shows a linear increase in ΔI at lower concentration and gradually a steady state is reached where no further increase in current was observed.

The BSA/anti-AFB_1/PEDOT-PSS-*f*MWCNTs/GCE showed linear response within two ranges of 0.1-25 $ngmL^{-1}$ and 30-55 $ngmL^{-1}$ towards the detection AFB_1 as shown in Figure 6.15 (A & B) with regression equation of linearity plot of given by:

$$\Delta I(\mu A) = 2.36\ \mu A ng^{-1} mL \times [AFB_1] + 0.011;\ R^2 = 0.99 \quad 6.11$$

$$\Delta I(\mu A = 0.307\ \mu A ng^{-1} mL \times [AFB_1] + 0.0573;\ R^2 = 0.99 \quad 6.12$$

The slope of linear fitting gives the sensitivity of 2.36 μAng-^{1}mL within the linear range of 0.1-25 ng/mL and 0.307 μAng^{-1}mL within linearity range of 30-55 ng/mL, respectively. The analytical performance of BSA/anti-AFB$_1$/PEDOT-PSS-*f*MWCNTs/GCE in maize sample spiked with different concentration of AFB$_1$ has been studied and Figure 6.16 shows the calibration plot with regression equation:

$$\Delta I(\mu A) = 8.89\,\mu Ang^{-1}mL \times [AFB_1] + 0.0466;\ R^2 = 0.99 \qquad 6.13$$

This corresponds to the sensitivity of 8.89 μAng^{-1}mL towards spiked maize sample within the linear range of 0.1 to 3 ng/mL. The limit of detection (LOD) and the limit of quantification (LOQ) were calculated from the parameters obtained from the regression curve, using LOD=3*S_y/s and LOQ=10*S_y/s, where 'S_y' is the standard deviation of the y-intercept and's' is the slope [446]. The analytical parameters of the synthesized electrode towards its analyte are presented in Table 6.7.

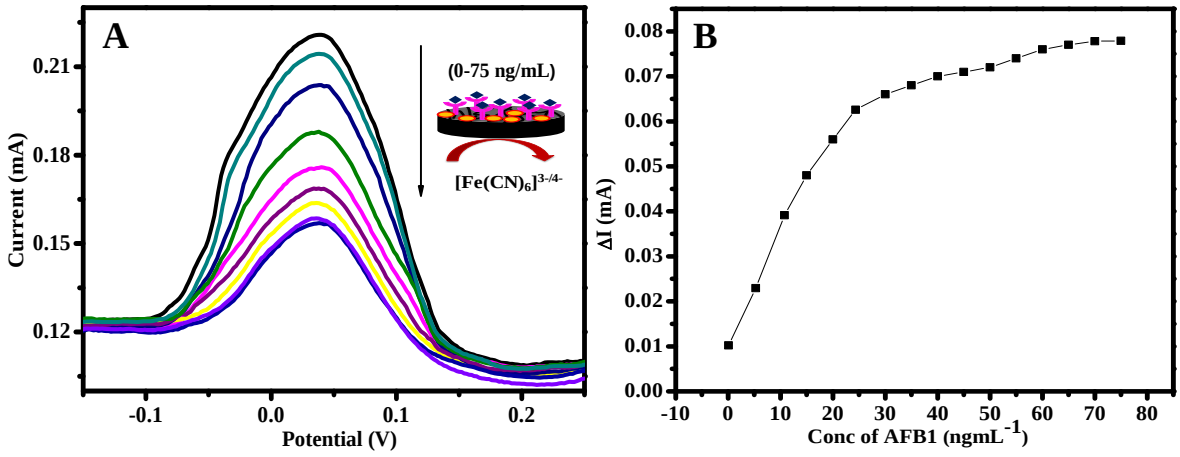

Figure 6.14: The DPV pattern of BSA/anti-AFB$_1$/PEDOT-PSS-*f*MWCNTs/GCE with concentration of AFB$_1$ (0-75 ng/mL) in 100mM PBS (pH 7.2) and 5mM [Fe (CN)$_6$]$^{3-/4-}$. (B) The Calibration plot of change in current (ΔI) vs. Concentration in ng/mL.

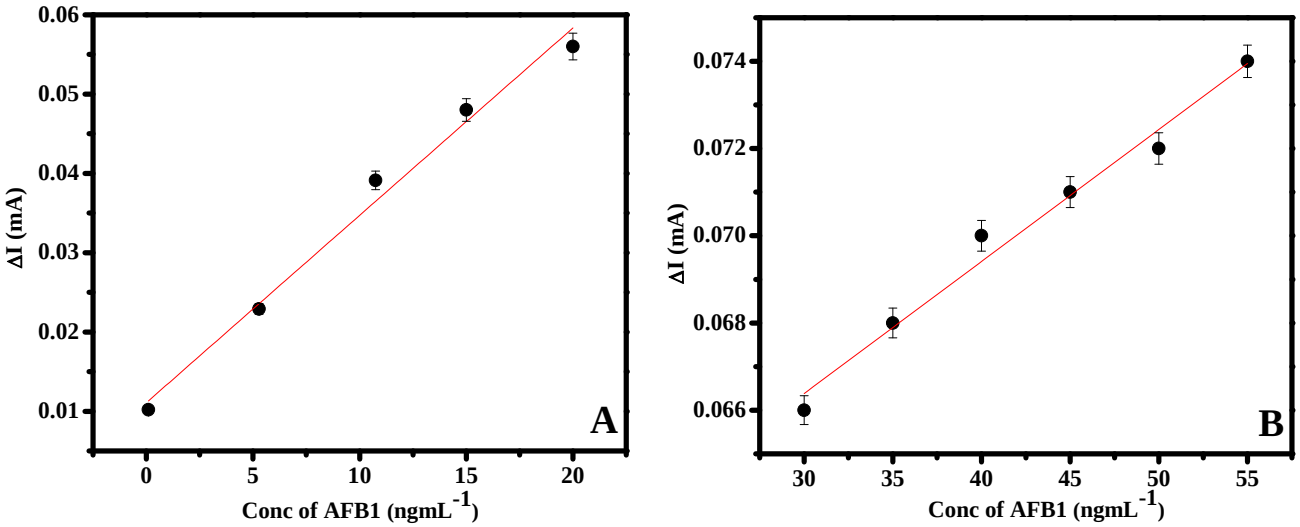

Figure 6.15: Linear slope of ΔI vs. Concentration in ng/mL of BSA/anti-AFB_1/PEDOT-PSS-*f*MWCNTs/GCE towards AFB_1.

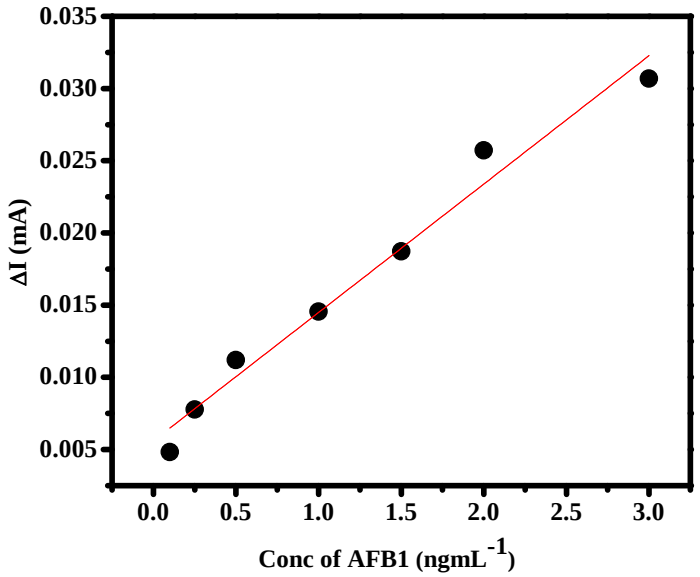

Figure 6.16: The linear response of the BSA/anti-AFB_1/PEDOT-PSS-*f*MWCNTs/GCE in varying concentration of AFB_1 in maize matrix.

Table 6.7: Analytical Parameters of the fabricated electrode towards the detection of AFB_1 in PBS and maize matrix.

Parameters	Values (in PBS)	Values (in maize matrix)
Linearity range (ng/ml)	0.5 to 20 ng/mL	0.1 to 3 ng/mL
Sensitivity	2.31 $\mu Ang^{-1}mL$	8.89 $\mu Ang^{-1}mL$
Correlation Coefficient (R^2)	0.99	0.98
LOD	0.491 ng/mL	0.123 ng/mL
LOQ	1.64 ng/mL	0.428 ng/mL

6.7.3 Specificity and recovery of BSA/anti-AFB_1/PEDOT-PSS-fMWCNTs/GCE towards real sample:

The applicability and practicability of the synthesized electrochemical immunosensor has been analyzed in AFB_1 spiked corn samples. The DPV results of BSA/anti-AFB_1/PEDOT-PSS-*f*MWCNTs/GCE in presence of corn sample spiked with 20 ng/mL and 40 ng/mL of AFB_1 is shown in Figure 6.17, respectively. The statistical calculation of standard addition method of spiked and unspiked samples (n=5) is tabulated in Tables 6.8 and 6.9. The recovery of the immunoelectrode towards AFB_1 in spiked corn sample and the average recoveries % $\left[\frac{measured\ value}{expected\ value} \times 100\right]$ is in the range of 97.67% and 96.45 % for 20 ng/mL and 40 ng/mL$^-$ concentration of AFB_1, respectively. The RSD (%) of recovery of the electrode for five consecutive measurements is found to be 0.35 and 0.55 for corn sample spiked with 20 ng/mL and 40ng/mL, respectively. Therefore the interference of other component and cross reaction of BSA/anti-AFB_1/PEDOT-PSS-*f*MWCNTs/GCE can be considered minimum indicating specificity of BSA/anti-AFB_1/PEDOT-PSS-*f*MWCNTs/GCE electrode towards AFB_1. Thus the electrode meets the requirement of ultra-sensitive detection of AFB_1.

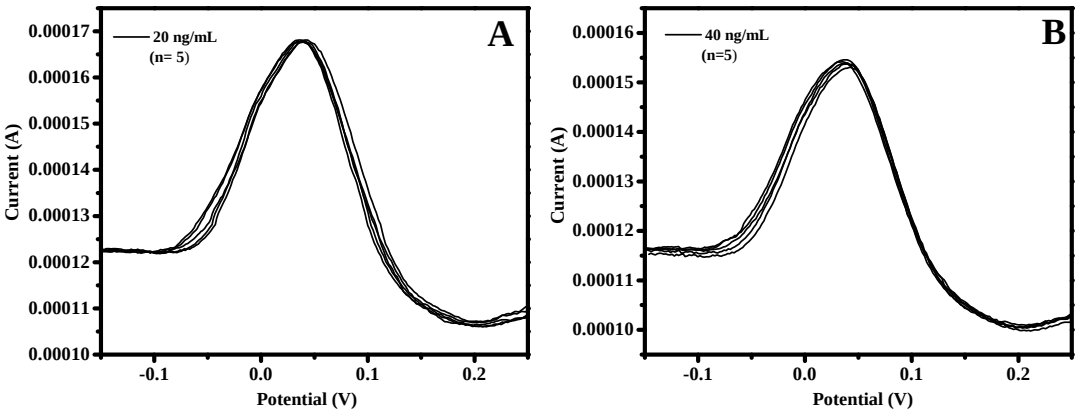

Figure 6.17: The DPV current variation of peak current of BSA/anti-AFB_1/PEDOT-PSS-*f*MWCNTs/GCE in 100 mM PBS (pH 7.4) and 5 mM $Fe(CN)_6^{3-/4-}$containing real corn sample spiked with (A) 20 ng/mL and (B) 40 ng/mL of AFB_1, respectively.

Table 6.8: Statistics and performance characteristics of BSA/anti-AFB_1/PEDOT-PSS-*f*MWCNTs/GCE towards standard AFB_1 sample.

Concentration of Aflatoxin B_1 (AFB_1)	**Measured Current (mA)**	**Average (x)**	**SD**	**RSD (%)**
20 ng/ml	0. 168	0.168	0.00957	0.569
	0.167			
	0.169			
	0.169			
	0.168			
40 ng/ml	0.154	0.155	0.000707	0.456
	0.155			
	0.155			
	0.156			
	0.155			

Table 6.9: Statistics and performance characteristics of the Working electrodes towards standard AFB_1 sample

Concentration of Aflatoxin Spiked (Conc of spiked/ standard AFB_1) (1:3)	**Measured Current (mA)**	**Average (x)**	**SD**	**RSD (%)**
20ng/ml	0. 166	0.164	0.000577	0.35
	0.164			
	0.164			
	0.165			
	0.165			
40ng/ml	0.152	0.150	0.000837	0.55
	0.150			
	0.151			
	0.151			
	0.150			

6.8 Application of BSA/anti-AFB_1/PEDOT-PSS-fMWCNTs/GCE to detect Methyl parathion and Carbofuran:

The detection principle of BSA/anti-AFB_1/PEDOT-PSS-*f*MWCNTs/GCE is based on monitoring the pesticide inhibition towards catalytic activity of AChE. Therefore the enzymatic activity of immobilized AChE has been first studied before the inhibition of pesticides.

6.8.1 Analytical behavior of BSA/anti-AFB_1/PEDOT-PSS-fMWCNTs/GCE towards Acetylthiocholine Chloride (AThCl):

The response of AChE/PEDOT-PSS-*f*MWCNTs/GCE towards AThCl has been investigated using CV and DPV technique. Figure 6.18 shows the CV pattern of AChE/PEDOT-PSS-*f*MWCNTs/GCE in absence and in presence of different concentration of AThCl. There is no noticeable peak in the CV pattern of AChE/PEDOT-PSS-*f*MWCNTs/GCE in absence of AThCl which depicts no electrochemical activity of bio-electrode in PBS solution. On addition of 1mM AThCl, an oxidation peak at around 0. 53 V vs. Ag/AgCl is seen which is due to oxidation of thiocholine (RSH) which is a product of hydrolysis of AThCl in presence of AChE [447]. The appearance of peak also infers that the AChE retains

its activity after immobilization over the matrix of PEDOT-PSS-*f*MWCNTs. The intensity of the peak at 0.53 V increases with increasing concentration of the AThCl denotes that the increasing enzymatic activity of AChE. The oxidation thicholine occurs at 0.5 V which is much lower than the oxidation potential of 0.7 V of thiocholine on solid matrices [369]. The enhancement of amperometric signal and the lowering of oxidation potential are attributed to the presence of *f*MWCNTs on the surface of GCE, which possessed a relatively large specific surface area and an inherent, high electricity conducting ability, thus they could enhance the rates of reactions as well as the electron transfer rate at a lower potential [448]. A reduction peak at around -0.45 V is due to the reduction of RSSR which is produced during anodic oxidation of thiocholine. The effect of changing scan rate on transfer of thiocholine species from solution to the electrode surface has been studied and it is displayed in Figure 6.19 (A). The linear variation of the anodic current with scan rate indicates the diffusion controlled process (Figure 6.19 (B)).

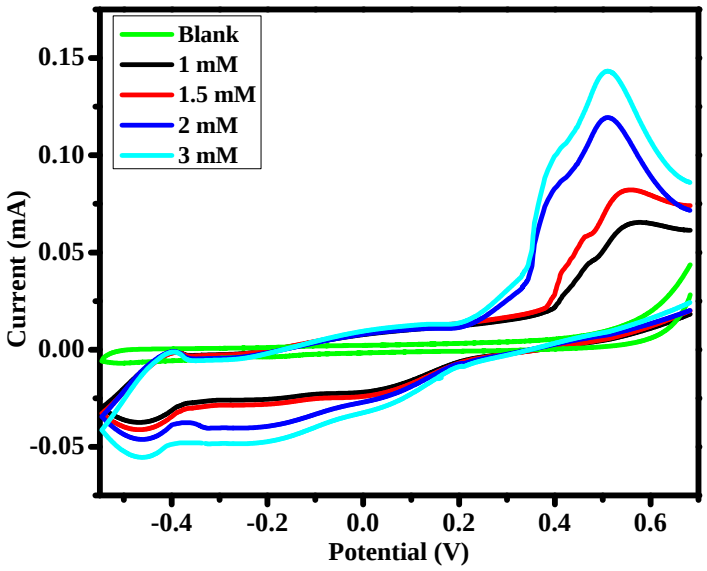

Figure 6.18: The cyclic voltammogram of AChE/PEDOT-PSS-*f*MWCNTs/GCE in 100mM PBS in absence and presence of different concentration of AThCl at a scan rate of 5mV/s vs. Ag/AgCl.

Enzyme kinetics have been further understood by DPV technique and the variation of DPV current peak of AChE/PEDOT-PSS-*f*MWCNTs/GCE in 100mM PBS with increasing concentration of AThCl ranging from 0.1 mM to 8 mM (Figure 6.20 (A)).

The intensity of current was found to be increasing initially and saturation occurs as we go on increasing the concentration of analyte which may be due to the blockage of active site of the enzyme at higher concentration of AThCl.

Figure 6.20 (B) shows the calibration plot (Michaelis-Menten) of the variation of DPV peak current of AChE/PEDOT-PSS-*f*MWCNTs/GCE vs. the concentration of the AThCl and the Figure 6.20 (C) is the Lineweaver Burk plot. The value of Michaelis Menten constant K_m has been calculated from lower linear part of calibration plot using equation [266]:

$$\frac{1}{i} = \frac{1}{I_{max}} + \frac{K_m}{I_{max}[AThCl]} \qquad 6.14$$

Where I_{max} corresponds to the saturation current of thiocholine oxidation and K_m is the Michelis Menten constant.

A lower value of K_m (~0.14 mM) and higher value of I_{max} (~412 μA) indicates an efficient affinity of immobilized AChE towards AThCl hydrolysis.

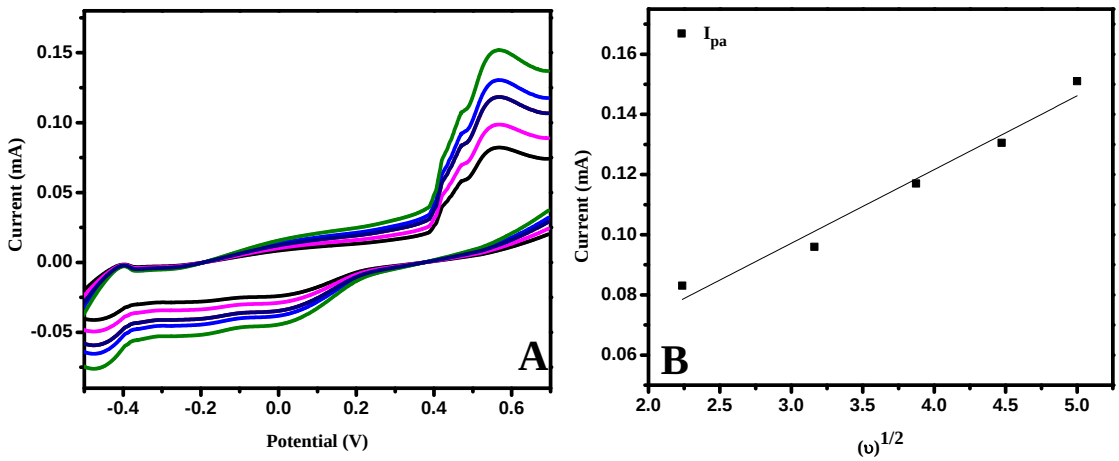

Figure 6.19: (A) The cyclic voltammogram of AChE/PEDOT-PSS-*f*MWCNTs/GCE in 100mM PBS and 2mM AThCl at different scan rate and (B) Linear variation of peak current (I_{pa}) vs. square root of scan rate ($\upsilon^{1/2}$).

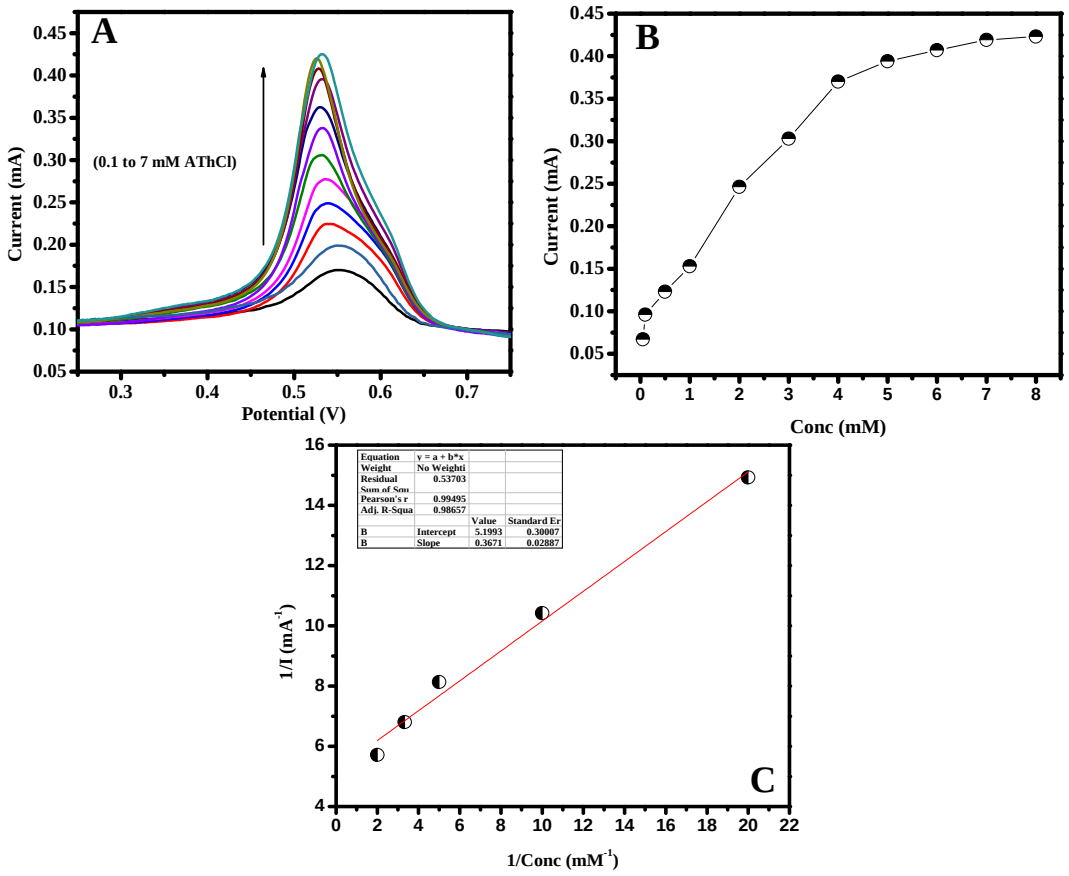

Figure 6.20: The DPV pattern of AChE/PEDOT-PSS-*f*MWCNTs/GCE in 100mM PBS and in presence of different concentration of AThCl, (B) Calibration Plot of Current vs. concentration of AThCl and (C) Lineweaver Burk Plot.

6.8.2 The effect of pH on electro-catalytic behavior of AChE/PEDOT-PSS-fMWCNTs/GCE:

The effect of pH on the electro chemical behavior of thiocholine species can be understood by plotting Pourbaix diagram between the peak potential E_{pa} and pH of the operating solution. The cyclic voltammetry of the AChE/PEDOT-PSS-*f*MWCNTs/GCE in presence of 2mM AThCl in 100mM PBS of different pH ranging from 6.5 to 8.5 is shown Figure 6.21 (A) and Figure 6.21 (B) shows the corresponding Pourbaix diagram. The oxidation potential shifts towards lower potential side with the increasing pH and shows a linear variation with regression equation of $E_{pa} = 0.056\,pH + 1.06$ with a slope of 56 mV/pH. This value is close to the theoretical value of 59 mV/pH calculated according to the Nernst equation

given by $pH = \frac{E_{pa}(V)}{0.059}$; this behavior indicates equal number of electron and proton transfer reaction [251].

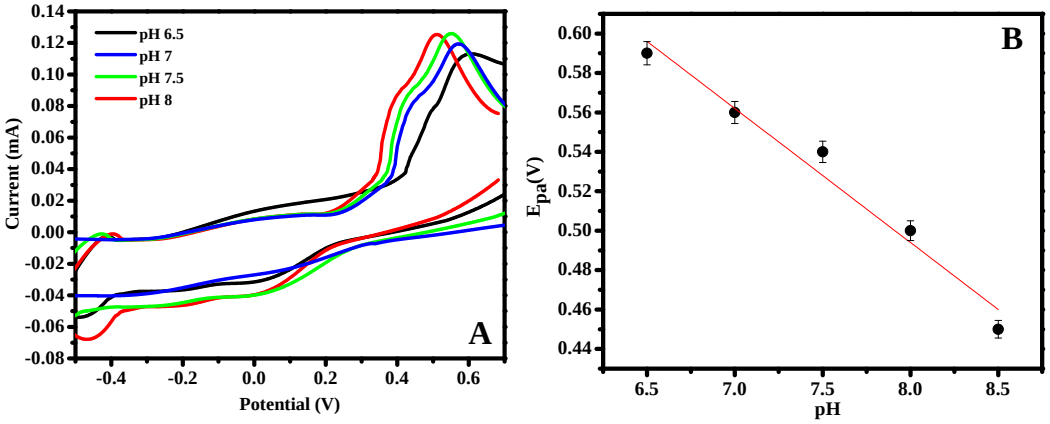

Figure 6.21: The CV of AChE/PEDOT-PSS-*f*MWCNTs/GCE in 2mM AThCl and 100mM PBS of different pH ranging 6.5 to 8.5 and (B) Plot of variation of the peak potential (E_{pa}) with pH of the solution.

6.8.3 Optimization of experimental parameters before pesticide inhibition:

Incubation time required for maximum inhibition of catalytic activity of AChE has been studied by measuring DPV in 100mM PBS and 2mM AChE after different incubation periods and the results are displayed in Figure 6.22. The pesticide inhibition on AChE activity at different incubation times ranging from 2 to 10 min was studied separately in 10 ng/mL of methyl parathion and carbofuran separately. The enzyme electrode, AChE/PEDOT-PSS-*f*MWCNTs/GCE showed a maximum decrease in DPV peak current value as a result of pesticides inhibition till incubation time of 6 min and 5 min, respectively. Therefore the optimized incubation time of 6 min and 5 min was fixed for the methyl parathion and carbofuran detection, respectively to get better sensitive pesticide biosensor.

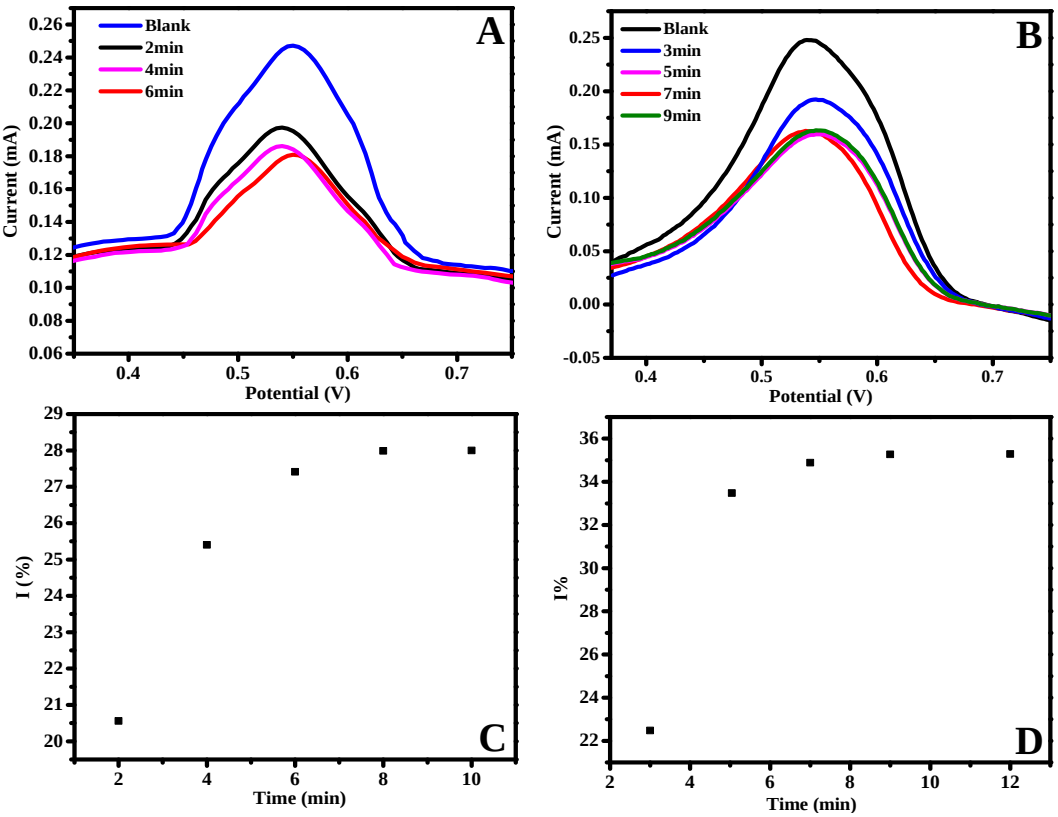

Figure 6.22: The DPV of AChE/PEDOT-PSS-*f*MWCNTs/GCE in 2mM AThCl and 100mM PBS in presence of (A) 10 ng/mL methyl parathion (B) 10 ng/mL carbofuran after different incubation time and (C & D) Plot of variation of the I (%) versus time in min.

6.8.4 Inhibition AChE/PEDOT-PSS-fMWCNTs/GCE in presence of methyl parathion:

The analytical performance of the synthesized AChE based biosensor towards methyl parathion and carbofuran was analyzed using DPV. The detection principle is based on measuring the DPV current in 2mM AThCl before pesticide inhibition (I_0) and after incubation with different concentration of pesticides (I_i). The DPV signal decreases intensely from 0.248 mA (Blank) to 0.0187 mA and 0.140 mA after the inhibition of carbofuran and methyl parathion, respectively.

The percentage of Inhibition (I%) and residual enzyme activities were calculated using equations (6.15) & (6.16) [415]:

$$Inhibition\ \%\ (I\%) = [(\frac{I_0 - I_i}{I_0}) \times 100] \qquad 6.15$$

$$Residual\ enzyme\ activity\ \%\ (REA\ \%) = \left[\frac{I_i}{I_0}\right] \times 100 \qquad 6.16$$

where I_0 and I_i is the measured DPV current in 2 mM AThCl and 100 mM PBS in absence and in presence of pesticides.

Figure 6.23 (A) shows the DPV peak current variation of the AChE/PEDOT-PSS-*f*MWCNTs/GCE in 100 mM PBS and 2mM AThCl in presence of varying concentration of carbofuran ranging from 1 ng/mL to 70 ng/mL after 5min incubation. The peak current varies inversely with the pesticide concentration as the formation of enzyme-inhibitor complex blocks the active sites of AChE [417]. The non-availability of active site of AChE results in poor hydrolysis of AThCl and this leads to less or no production of thiocholine and hence the peak current decreases. In presence of carbofuran, AChE/PEDOT-PSS-*f*MWCNTs/GCE showed linearity in two ranges 0.1-30 ng/mL and 30-50 ng/mL with regression equation of $I(\%) = 1.33\ [AThCl] + 9.9$ and $I(\%) = 1.87\ [AThCl] + (-4.86)$ with regression coefficient of 0.99 and 0.998, respectively. The LOD and LOQ of 0.073 ng/mL and 0.245 ng/mL were found towards the detection of carbofuran in the linear range of 0.1 to 30 ng/mL, respectively. The analytical performance of the biosensor towards different concentration of methyl parathion is displayed in Figure 6.24. The biosensor showed a linearity of 0.1 to 20 ng/mL and 20 to 40 ng/mL towards the inhibition of Methyl Parathion with regression equation of $I(\%) = 1.169\ [AThCl] + 12.01$ and $I(\%) = 0.46\ [AThCl] + 24.29$ with regression coefficient of 0.95 and 0.99, respectively. The electrode showed a small detection and quantification limit of 0.212 ng/mL and 0.707 ng/mL, respectively which signifies the efficient detection of pesticides.

After exposure of the immobilized enzyme to the pesticide samples, the fraction of enzyme that avoided inhibition has been calculated using equation 6.16 and Figure 6.26 (A & B) shows the calibration plot of residual enzyme activity (%) vs. the concentration of the pesticides. As the pesticides sample concentration increases the residual activity decreases with time. In presence of carbofuran, more enzymes succumb to inactivation and 10% enzymes remains active after inhibition of 70 ng/mL of carbofuran. On the other hand, 53 % of enzyme remains active after inhibition of methyl parathion. The results indicate that the bioelectrode

AChE/PEDOT-PSS-*f*MWCNTs/GCE is an efficient sensor for the detection of the individual pesticides.

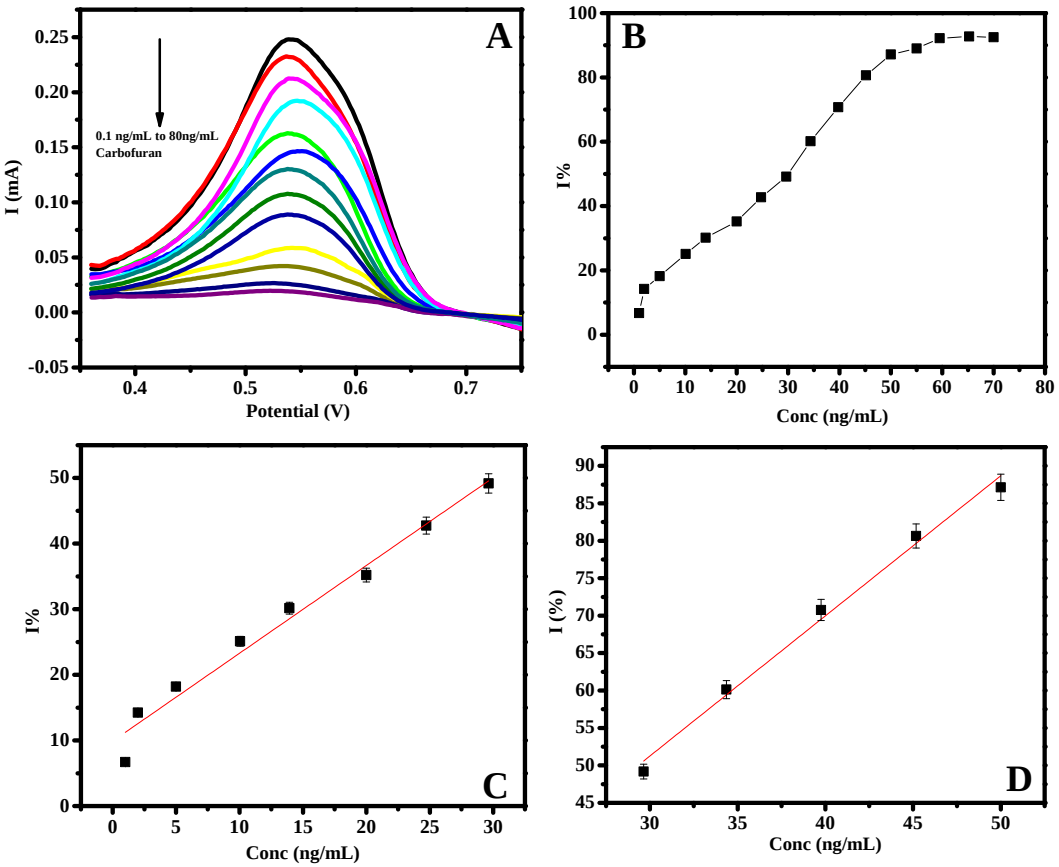

Figure 6.23: (A) The DPV peak variation of AChE/ PEDOT-PSS- *f*MWCNTs after inhibition of different concentration of carbofuran in 100 PBS and 2mM AThCl; (B) The calibration plot of inhibition (I%) vs. concentration of carbofuran in ng/mL; (C & D) The linearity range of I % vs. concentration of carbofuran.

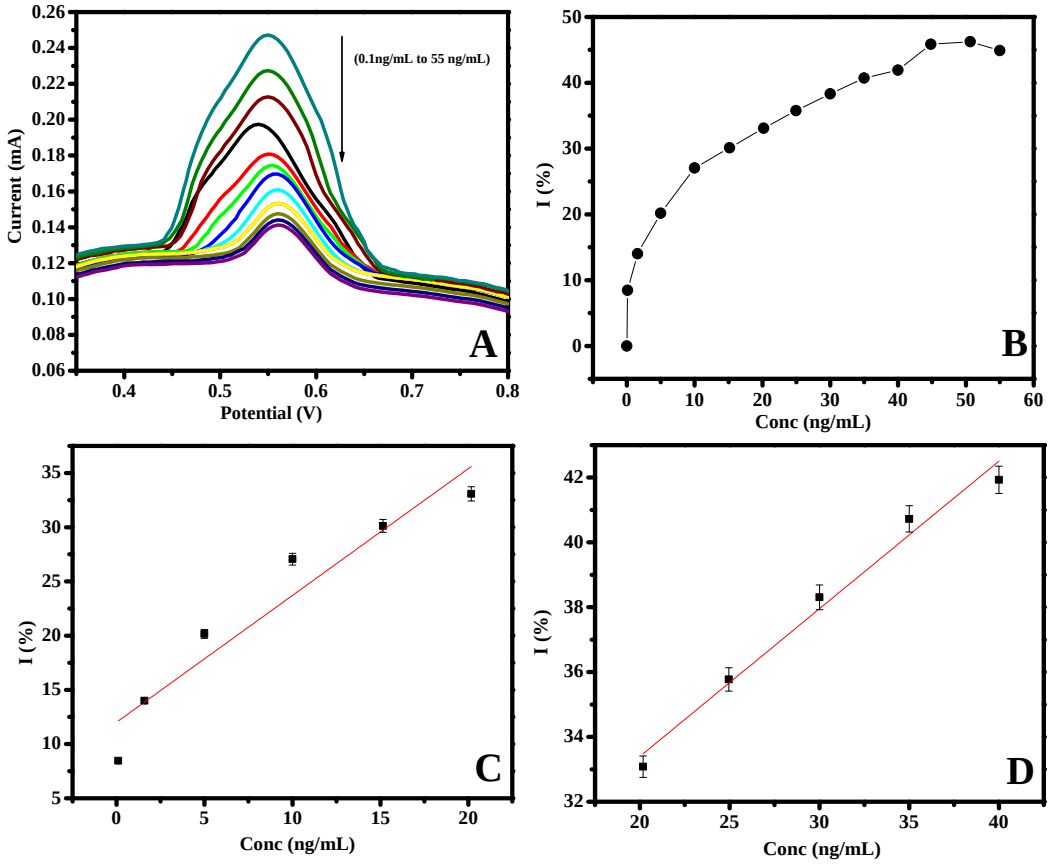

Figure 6.24: (A) The DPV peak variation of AChE/PEDOT-PSS- *f*MWCNTs after inhibition of different concentration of methyl Parathion in 100 PBS and 2mM AThCl; (B) The calibration plot of inhibition (I%) vs. concentration of methyl Parathion in ng/mL; (C & D) The linearity range of I % vs. concentration of methyl Parathion.

The analytical parameters towards the response of carbofuran and methyl parathion have been tabulated in Table 6.10. The shelf life and operational stability of the AChE/PEDOT-PSS-*f*MWCNTs/GCE electrode has been studied (Figure 6.27) and found that the biosensor showed a consistent behavior towards its analyte and there is 90 % recovery in the amperometric signal till 210 days when stored in phosphate buffer at 15^0C.

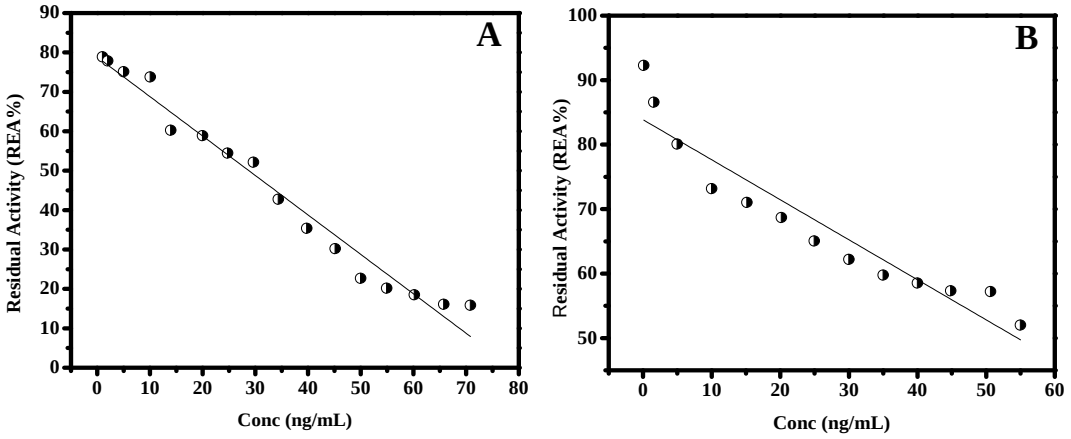

Figure 6.25: The residual activity of the AChE/PEDOT-PSS-*f*MWCNTs/GCE towards different concentration of (A) Carbofuran and (B) Methyl Parathion respectively.

Table 6.10: Analytical parameters of AChE/PEDOT-PSS-*f*MWCNTs/GCE towards the detection of Methyl parathion and Carbofuran

Parameters	**Towards Methyl Parathion**	**Towards Carbofuran**
Linearity	0.1- 20 ng/mL; 20-40 ng/mL	0.1-30 ng/mL; 30-50 ng/mL
Sensitivity (inhibition per concentration in ng/mL)	1.169 $ng^{-1}mL$ 0.46 $ng^{-1}mL$	1.33 $ng^{-1}mL$ 1.87 $ng^{-1}mL$
Correlation Coefficient (R^2)	0.95; 0.99	0.96; 0.98
LOD	0.212 ng/mL	0.073 ng/mL
LOQ	0.707 ng/mL	0.245 ng/mL

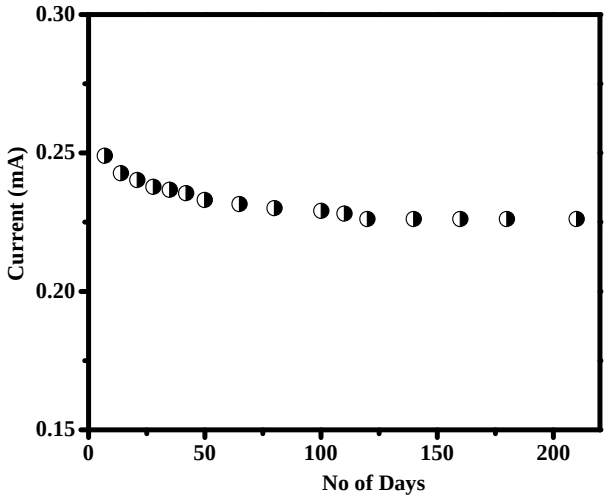

Figure 6.26: Shelf life study and the activity of the immobilized AChE in PEDOT-PSS-*f*MWCNTs/GCE towards the hydrolysis of AThCl.

6.8.5 Inhibition AChE/PEDOT-PSS-fMWCNTs/GCE in presence of real sample spiked with methyl parathion and carbofuran:

The feasibility of AChE/PEDOT-PSS-*f*MWCNTs/GCE in presence of real sample has been studied further by measuring the amperometric signal in presence of real samples spiked with pesticides. Figure 6.28 (A & B) presents the DPV peak current of the AChE/PEDOT-PSS-*f*MWCNTs/GCE in 100 mM PBS and 2 mM AThCl after inhibition in 3 mL of soil water spiked with 10 ng/mL methyl parathion and carbofuran, respectively. Table 6.11 (A & B) shows the value of the current obtained and expected for each concentration (n=3) and the synthesized bio-electrode exhibits a good recovery of 93.51 % and 100.5 % towards soil water samples spiked with methyl parathion and carbofuran, respectively.

The practicability of AChE/PEDOT-PSS-*f*MWCNTs/GCE has been further tested by using green tea sample spiked with 10 ng/mL methyl parathion and carbofuran. The DPV measurements (n=3) and the statistical calculation have been displayed in Figure 6.29 (A & B) and Table 6.12 (A & B), respectively. An excellent recovery of 97.79 % and 98.63 % has been found in presence of green tea water samples spiked with methyl parathion and carbofuran, respectively. Therefore the synthesized AChE based bioelectrode can be considered as a suitable matrix for designing devices for field applications.

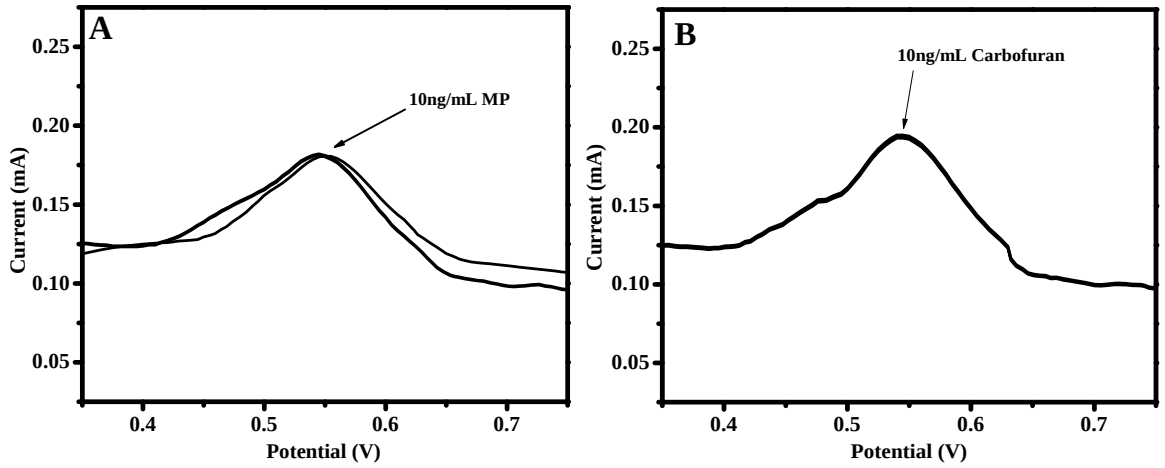

Figure 6.27: The DPV signal of AChE/PEDOT-PSS-*f*MWCNTs/GCE in absence and presence of soil water spiked with 10 ng/mL of MP and 10 ng/mL of carbofuran.

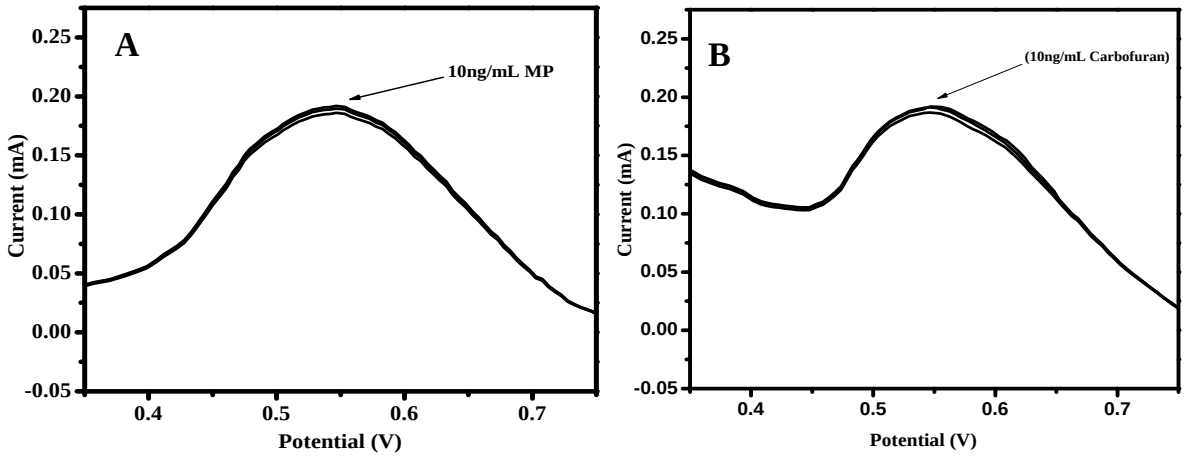

Figure 6.28: The DPV signal of AChE/PEDOT-PSS-*f*MWCNTs/GCE in absence and presence of green tea water spiked with 10 ng/mL of MP and 10 ng/mL of carbofuran.

Table 6.11: Statistics and performance characteristics of the AChE/PEDOT-PSS-fMWCNTs/GCE towards soil water sample spiked with pesticide sample:

(a) 10ng/mL of carbofuran:

Expected value (mA)	Measured value (mA)	Average	Inhibition	Recovery (%)
0.197	0.181	0.183	21 %	93.12
0.196	0.183			
0.196	0.185			

(b) 10ng/mL of methyl parathion:

Expected value (mA)	Measured value (mA)	Average	Inhibition	Recovery (%)
0.197	0.190	0.192	21 %	97.79
0.196	0.193			
0.196	0.195			

Table 6.12: Statistics and performance characteristics of the AChE/AuNPs/PEDOT-GO/GCE towards green tea water sample spiked with pesticide sample

(a) 10ng/mL of carbofuran:

Expected value (mA)	Measured value (mA)	Average	Inhibition	Recovery (%)
0.192	0.195	0.193	22 %	100.51
0.191	0.190			
0.192	0.192			

(b) 10ng/mL of methyl parathion:

Expected value (mA)	Measured value (mA)	Average	Inhibition	Recovery (%)
0.192	0.191	0.189	23.7 %	98.43
0.191	0.190			
0.192	0.186			

6.9 Summary:

A nanohybrid composite of PEDOT-PSS-*f*MWCNTs has been synthesized by electrochemical oxidation of EDOT in presence of PSS and *f*MWCNTs. The anti-AFB_1 and AChE was immobilized over the matrix of PEDOT-PSS-*f*MWCNTs probe using carbodiimide crosslinking between the COOH group of PEDOT-PSS-*f*MWCNTs and NH_2 group of the proteins. The surface morphology of the synthesized films shows a rough surface and a porous network of PEDOT-PSS film. In PEDOT-PSS-*f*MWCNTs the nanotubes of thickness ca. 5nm are found to be wrapped in the growing polymer and an interconnected network of incorporated nanotubes may have formed. The increase in surface hydrophilicity (ca~44^0) is due to the presence of hydrophilic functional groups in PEDOT-PSS-*f*MWCNTs composite. Fundamental stretching vibrations of all the synthesized composite films have been assigned in FTIR spectra. Presence of primary amine band between 1600-1650 cm^{-1} confirms that the proteins retain their native state after immobilization. The activation barrier to the flow of electrons is found to be minimum for PEDOT-PSS-*f*MWCNTs/GCE with R_{et}~140 Ω, thus the presence of *f*MWCNTs may generate nano channels for successful electron transfer by increasing interfacial catalytic active sites between PEDOT-PSS-*f*MWCNTs/GCE electrode and the redox active solution ($Fe[(CN)_6]^{3-/4-}$). The EIS results are corroborated with the cyclic voltammetry results as the PEDOT-PSS-*f*MWCNTs/GCE shows an improved electrochemical behavior with peak current intensity of 169 μA and -168 μA (ΔE_p ~ 69mV) towards the redox species. The large surface area of the nanotubes ($1315 m^2/g$ (theoretical value)) contributes to a dramatic increase in electro active area of GCE from 0.08 cm^2 to 0.818 cm^2 which results in large embedding of protein molecules on the order 10^{-5} mol/cm^2. The mean k_s value of 1.8×10^2 s^{-1} for PEDOT-PSS-*f*MWCNTs/GCE indicates fast kinetics of the redox couple which may be attributed

to the highly conducting carbon nanotubes network incorporated in the polymer matrix. The value of k_s after immobilization of proteins is found to be on order of 10^{-2} which suggests that the electron transfer pathway of the protein behaved as a quasi-reversible system.

The immunosensing experiments of BSA/anti-AFB_1/PEDOT-PSS-*f*MWCNTs/GCE have been performed in optimized condition of operating pH 7.2 and incubation time of 5 min. The synthesized electrode shows linear response within two ranges of 0.1-25 ng/mL and 30-55 ng/mL towards the detection AFB_1 with a high sensitivity of 2.36 μAng-^{1}mL in the linear range of 0.1-25 ngmL^{-1} and of 0.307 μAngmL^{-1} in the linearity range of 30-55 ng/mL. The minimum concentration of AFB_1 that can be detected and quantified were found to be 0.491 ng/mL and 1.64 ng/mL, respectively. An excellent sensitivity of 8.89 μAngmL^{-1} towards spiked maize sample has been determined with LOD and LOQ of 0.128 ng/mL and 0.428 ng/mL, respectively. The interference of other component and cross reaction of BSA/anti-AFB_1/PEDOT-PSS-*f*MWCNTs/GCE can be considered minimum as the electrode showed a recovery of ca 98% in presence of real corn sample.

The AChE based biosensors AChE/PEDOT-PSS-*f*MWCNTs/GCE can be considered as an efficient platform for thiocholine oxidation as the oxidation potential of thiocholine decreases from 0.8 V to 0.55V vs. Ag/AgCl. The enhancement of amperometric signal and the lowering of oxidation potential are attributed to the presence of *f*MWCNTs on the surface of GCE, which possessed a relatively large specific surface area and an inherent, high electricity conducting ability, thus they could enhance the rates of reactions as well as the electron transfer rate at a lower potential. The enhanced enzymatic activity of the immobilized AChE can be further explained by the small K_m value of 0.14mM and a high value of I_{max} showed efficient affinity of AChE towards AThCl.

In presence of carbofuran, AChE/PEDOT-PSS-*f*MWCNTs/GCE showed linearity in two ranges 0.1-30 ng/mL and 30-50 ng/mL with LOD and LOQ of 0.073 ng/mL and 0.245 ng/mL, respectively. Similarly the analytical performance of the biosensor towards different concentration of methyl parathion was studied and bioelectrode showed a linearity of 0.1 to 20 ng/mL and 20 to 40 ng/mL towards the inhibition of Methyl Parathion. A small detection and quantification limit of 0.212 ng/mL and 0.707 ng/mL, respectively signifies an efficient detection of pesticides.

The shelf life and operational stability of the AChE/PEDOT-PSS-*f*MWCNTs/GCE electrode has been studied and the biosensor showed a consistent behavior towards its hydrolysis of its analyte and there is 90 % recovery in the amperometric signal till 210 days when stored in phosphate buffer at 15^0C.